J. Phys. F: Met. Phys. **15** (1985) 111–139. Printed in Great Britain

A unified approach to residual resistivity, thermoelectric power, ultraviolet photoelectron spectroscopy and de Haas–van Alphen measurements on dilute CuNi, CuPd, CuRh and CuPt alloys

J A Julianus†‖, A Myers‡, F F Bekker†, D van der Marel§ and E F Allen‡

† Natuurkundig Laboratorium der Universiteit van Amsterdam, Valckenierstraat 65, 1018 XE Amsterdam, The Netherlands

‡ Department of Physics, University of Leeds, Leeds LS2 9JT, UK

§ Physical Chemistry Department of the Material Science Centre, University of Groningen, Nijenborgh 16, 9747 AG Groningen, The Netherlands

Received 11 May 1984, in final form 16 July 1984

Abstract. Measurements have been made of the residual resistivity and thermoelectric power in dilute alloys of **Cu**Ni, **Cu**Pd, **Cu**Pt and **Cu**Rh. A measurement has also been made of the UPS spectrum in **Cu**Rh. These have been used to obtain the parameters associated with the resonant d states in these alloys using the phase-shift model of Gupta and Benedek. De Haas–van Alphen measurements made by other workers have been re-analysed, using the new residual resistivities, within the phase-shift model of Coleridge, Holzwarth and Lee. Comparison is made between the parameters obtained from these two approaches. Various theoretical calculations of the de Haas–van Alphen Dingle temperature and frequency change on alloying are discussed in relation to the measured values.

1. Introduction

Over the last decade impressive progress has been made in the theory of dilute aloys. For example, the systematic band calculations of Moruzzi *et al* (1978) for perfect metals have been extended by Zeller and Dederichs (1979) to the calculation of the local density of states for dilute alloys using the same density functional theory in the local spin density approximation. In Cu- and Ag-based dilute alloys with 3d and 4d elements, traditional virtual bound-state (VBS) systems in the Friedel–Anderson sense (Friedel 1958, Anderson 1961), a more realistic theoretical picture is developing (Zeller *et al* 1980, Podloucky *et al* 1980, Braspenning *et al* 1984). (For example, the number of electrons taken to be in the peak now includes the contribution from the local density of states of the host d band.) This was the background to the present work in which direct measurements of the electron density of states using ultraviolet photoelectron spectroscopy (UPS) are related to the indirect information about the resonant d state obtained from the residual resistivity, thermoelectric power (TEP) and de Haas–van Alphen (DHVA) Dingle temperature and frequency change (see figure 1).

As far as the analysis of the experimental results is concerned, DHVA measurements, which provide information about the scattering anisotropy over the Fermi surface, can be

‖ Present address: North-Holland Publishing Co., Molenwerf 1, PO Box 1991, 1000 BZ Amsterdam, The Netherlands.

0305-4608/85/010111 + 29 $02.25

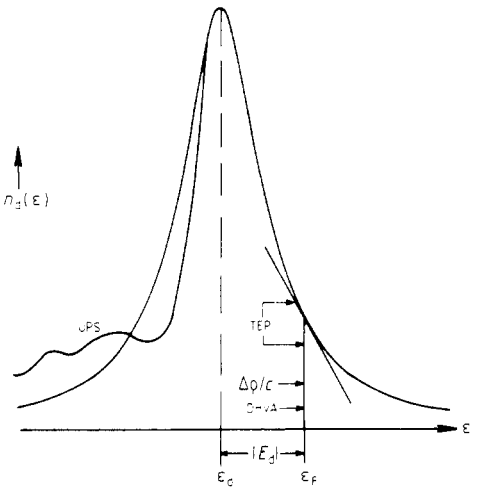

Figure 1. Schematic picture of unified approach to $\Delta\rho/c$, TEP, UPS and DHVA measurements.

analysed using a model developed by Coleridge *et al* (1974, hereafter referred to as CHL) based on a KKR treatment of phase-shift scattering and making use of a parametrisation of the host Fermi surface. The DHVA data for **Cu**Pd, **Cu**Pt and **Cu**Rh of Coleridge *et al* (1981, hereafter referred to as CTT) were originally analysed by them to give the effective (or Friedel) scattering phase shifts (φ_l^{CHL}); in this analysis the resistivity of the alloy was needed. In the present work significantly different resistivities from those used by CTT are found and the DHVA data have been re-analysed, this time using a graphical method of solution (see, e.g., Julianus *et al* 1984b). The CHL model includes the residual resistivity but the problems of extending it to include the TEP have not yet been overcome. The TEP therefore cannot be analysed within the CHL model, but it can be analysed together with the residual resistivity in terms of a model developed by Gupta and Benedek (1979, hereafter referred to as GB). This model incorporates both the Bloch-wave character of the electron states and backscattering but it is simpler than the CHL model, integrations over the Fermi surface being avoided since a spherical band approximation is used. The TEP is analysed within the GB model using the information derived from the UPS measurements and sets of effective phase shifts (φ_l^{GB}) are obtained.

Both the GB model and the CHL model are based on a muffin-tin approximation and the impurity is described by a single muffin-tin potential. Neither model allows for lattice distortion or charge transfer. Recent cluster calculations (Molenaar *et al* 1983, Molenaar and Lodder 1983, Braspenning *et al* 1984) incorporate these effects and have been made (Lodder 1983) for **Cu**Ni, **Cu**Pd and **Cu**Rh for DHVA Dingle temperatures and frequency changes. A comparison of these calculated quantities with the corresponding quantities measured by CTT, Poulsen *et al* (1974) and Templeton and Coleridge (1975) indicates the significance of charge-transfer effects in these systems.

In summary, in the present work measurements are presented of the electrical resistivity and the TEP in dilute **Cu**Ni, **Cu**Pd, **Cu**Pt and **Cu**Rh alloys; measurements are also presented of the UPS lineshape in **Cu**Rh. UPS measurements already exist for the other alloys (Bosch *et al* 1984, van der Marel *et al* 1985). The resistivity and TEP analysis is made within the GB model. In addition, DHVA measurements on these alloys made previously by a number of workers are re-analysed using the new values for the resistivity; this analysis is made within the CHL model. Comparison is made between the sets of phase

shifts obtained from the GB and CHL models and a comparison is also made between the experimental data and corresponding values obtained from theoretical calculations.

2. Experiment

2.1. Sample preparation and resistivity

Considerable care was taken in the preparation of the alloys both for residual resistivity and for TEP measurements. In the case of the residual resistivity the important factor is to have the solute fully in solution. Myers *et al* (1980) showed how the resistivity in **Au**Rh could be changed dramatically by the effect of the heat treatment. As far as the TEP is concerned, it is well known that iron as an impurity in solution affects the TEP profoundly.

The copper alloys were made by melting together weighed quantities of the solvent, Cu, and the solute in a quartz tube filled to approximately one third of an atmosphere with argon using inductive heating. The alloys were heated to 1200 °C for about 30 min before being quenched in distilled water. They were then rolled to give three rods of dimensions approximately $200 \times 1 \times 1$ mm^3, surface contamination being minimised by immersion in boiling HCl between each rolling operation. The rods were annealed in vacuo at approximately 950 °C and were then quenched in distilled water. Some of the alloy taken from the ends of the resistance rods was analysed chemically using atomic absorption techniques. The TEP samples were prepared from the resistance rods by using diamond dies to give a wire of final diameter 0.3 mm.

The starting materials were copper of 99.9999% purity and transition metals of at least 99.999% purity. Despite the precautions taken some problems with iron contamination were encountered.

The residual resistances were measured using a conventional four-terminal technique.

2.2. Thermoelectric force

The measurements of the thermoelectric force (TEF) were carried out in a conventional ^{4}He cryostat using a semi-automatic system. One end of the wire sample was kept at a constant temperature, $T_b = 1.5$ K, whereas the other end was heated in steps of 0.1–0.3 K between 1.6 and 16 K. The temperature of the heated end was measured with a calibrated Ge resistor. The thermoelectric force was measured in this temperature range against a superconducting Nb_3Sn reference strip, a superconducting switch being used to eliminate spurious thermoelectric effects. The voltage across the sample was compensated by adjusting the current through a resistor at temperature T_b using a Keithley 148 nanovoltmeter as the null detector. The accuracy was typically about 1 nV. A detailed description of the semi-automatic equipment has been given recently by Julianus *et al* (1984a).

2.3. Ultraviolet photoelectron spectroscopy

The UPS spectra were recorded in an angle-integrated mode using He I radiation of 20.22 eV. A detailed description of the equipment, which had an overall resolution of 85 meV at 10 eV pass energy, has been given elsewhere (Bosch 1982). The base pressure in the apparatus was less than 10^{-10} Torr and the samples, which had been polished mechanically prior to insertion in the vacuum chamber and then etched with 1 keV Ar^+

ions, gave a spectrum which did not deteriorate noticeably over a period of 30 min. The effect of Ar^+ ion bombardment on the surface composition of the polycrystalline samples was checked with XPS. After preparation of an oxygen-free surface there was no evidence of preferential sputtering affecting the solvent/solute concentration, indicating either that this did not occur or that the bulk composition was quickly restored by diffusion at room temperature.

3. Results

3.1. Resistivity

The residual resistivity, $\Delta\rho$, was analysed according to the relation

$$\Delta\rho = qc + pc^2 + r \tag{1}$$

where c is the concentration. Least-squares fits based on (1) showed that r was negligible for all systems, and that only in the case of **Cu**Pd was the squared term significant. The results are summarised in table 1, together with data from earlier measurements and the values used by CHL, Templeton and Coleridge (1975) and CTT in their analyses of the DHVA data. The least-squares fits to the data are shown in figure 2.

The value found for **Cu**Ni is in good agreement with earlier measurements (see table 1). In the case of **Cu**Pd, CTT used a value for the resistivity of 0.89 $\mu\Omega$ cm (at.%)$^{-1}$ obtained from the results of Linde's (1932) measurements at room temperature which are obviously less satisfactory than low-temperature measurements. A value for the low-temperature resistivity obtained by CTT using nominal concentrations was 0.80 $\mu\Omega$ cm (at.%)$^{-1}$, which is very close to our value of 0.82 $\mu\Omega$ cm (at.%)$^{-1}$ and the value of 0.84 $\mu\Omega$ cm (at.%)$^{-1}$ obtained by Kierspe (1967). The latter results also show some evidence for deviations from Matthiessen's rule. For **Cu**Pt we found a higher resistivity than CTT used; they again adopted the results of Linde (1939). For **Cu**Rh we also found a higher resistivity than CTT; in this case they deduced a resistivity of 3.57 $\mu\Omega$ cm (at.%)$^{-1}$ following chemical analysis of their DHVA specimens. In this alloy the accurate measurements of Loegel (1973)

Table 1. Summary of residual resistivity data. p and q are the least-squares fitting parameters in (1). σ is the standard deviation, N the number of data points and c_{max} is the highest concentration of the samples included in the fit.

	q ($\mu\Omega$ cm (at.%)$^{-1}$)						
Alloy	This work	Other workers	DHVA†	p ($\mu\Omega$ cm (at.%)$^{-2}$)	σ ($\mu\Omega$ cm)	N	c_{max} (at.%)
CuNi	1.106 ± 0.004	1.138[b] 1.112[c]	1.11[f]		0.056	29	5.5
CuPd	0.82 ± 0.01	0.84[d]	0.89[e]	−0.012 ± 0.003	0.048	23	5.2
CuPt	2.24 ± 0.03	1.86[d]	2.10[e]		0.185	15	3.2
CuRh	4.03 ± 0.06	4.03[a]	3.57[e]		0.35	20	2.8

[a] Loegel (1973); [b] Lengeler *et al* (1970); [c] Legvold *et al* (1974); [d] Kierspe (1967); [e] Coleridge *et al* (1981); [f] Coleridge *et al* (1974), Templeton and Coleridge (1975).

† Residual resistivity values used previously to analyse DHVA data.

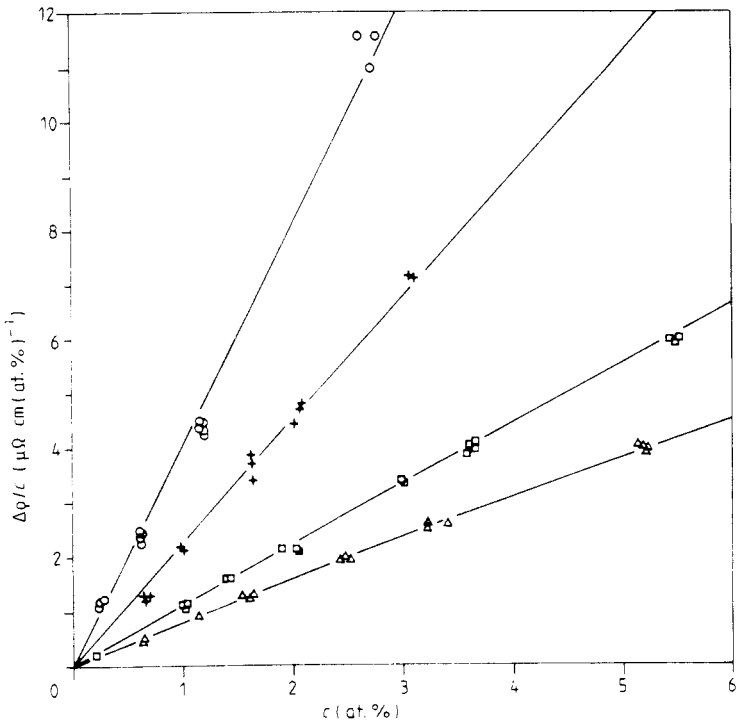

Figure 2. Plot of $\Delta\rho$ against concentration for **Cu**Pd (△), **Cu**Ni (□), **Cu**Pt (+) and **Cu**Rh (○). The full lines are least-squares fits to the data based on (1) with the parameters shown in table 1.

give strong support for our findings. The low resistivity value for **Cu**Pt as obtained by Kierspe (1967) is from three data points, all taken at concentrations below 3 at.% Pt.

In summary, we have confidence in our residual resistivity values not only because of the support from measurements of other workers, but especially considering (i) that the concentrations of our samples were determined by chemical analysis instead of relying on nominal concentrations, (ii) that the alloys were given a careful heat treatment to have the solute fully in solution and (iii) the good statistics of our data (at least 15 data points, small standard deviations). Since our values differ significantly from those used by CTT in their analysis of the DHVA data in all alloys except **Cu**Ni, a renormalisation of the DHVA results of CTT is justified.

3.2. Thermoelectric force

Least-squares fits to the TEF, $E^T_{T_b}$, measured between the bath temperature T_b and the adjustable temperature T, of the form

$$E^T_{T_b} = -E_0^{T_b} + CT[1-(T_0/T)\ln[1+(T/T_0)]] + \tfrac{1}{2}P_1T^2 + \tfrac{1}{4}P_3T^4 \qquad (2)$$

are applied using data points $(T, E^T_{T_b})$ below $T=\theta$; θ is varied in steps of 1 K and the upper limit to θ is established on the basis of the standard deviation σ_θ $(=\Sigma_i\,[\varepsilon_i^2/(N_\theta - M)]^{1/2}$ where ε_i is the difference between the fitted curve and data point i, N_θ is the number of data points below $T=\theta$ and M is the number of parameters). A detailed description of the background to (2) has been given by Julianus *et al* (1984a). Briefly, the first term is an integration

Table 2. TEP data on **CuNi**, **CuPd**, **CuPt** and **CuRh** alloys. c_{Fe} is calculated from the value of C using the Nordheim–Gorter rule. The value of A is the average of the values of P_1 for each system.

Solute	c (at.%)	$\Delta\rho$ ($\mu\Omega$ cm)	θ (K)	P_1 (nV K^{-2})	$10^3 P_3$ (nV K^{-4})	C (nV K^{-1})	c_{Fe} (PPM)	σ_θ (nV)	N_θ
Ni	1.03	1.18	13	-66.36 ± 0.08		-2.3 ± 0.8	0.12 ± 0.04	1.6	25
Ni†	1.03		4	-65.6 ± 0.2	$+38 \pm 23$	1.5	0.08	0.4	17
Ni	2.03	2.16	14	-68.9 ± 0.1		-3.9 ± 1.2	0.36 ± 0.11	2.7	25
Ni	3.02	3.37	9	-68.9 ± 0.4		-114 ± 4	16.6 ± 0.6	2.9	16
				$A = -67.4 \pm 1.6$					
Pd	1.61	1.29	6	-10.7 ± 3.2	-11 ± 45	-157.6 ± 17.5	8.8 ± 1.0	1.14	20
Pd	2.47	1.96	7	-7.63 ± 1.75	-23 ± 20	-157 ± 10	14.9 ± 0.9	1.07	20
Pd	3.42	2.63	10	-7.63 ± 0.31	-16 ± 2	-2.8 ± 2.1	0.32 ± 0.24	0.74	32
Pd	5.18	3.96	8§	-6.7 ± 1.7	-12 ± 16	-109 ± 10	18.6 ± 1.7	1.24	14
				$A = -8.2 \pm 2.7$					
Pt	0.99	2.22	6	-8.72 ± 0.14‡	-33 ± 8			0.98	19
Pt†	0.99		8§	-9.06 ± 0.06	$+43 \pm 2$			0.93	22
Pt	2.10	4.82	6	-9.73 ± 0.11	-21 ± 6			0.79	18
Pt	3.09	7.19	6	-9.72 ± 1.97	-17 ± 27	-2.6 ± 10.7	< 4.1	0.71	24
				$A = -9.5 \pm 1.3$					
Rh†	0.62_5	(2.95)	5	-27.12 ± 0.15	$+65 \pm 12$			0.65	17
			11	$-25.7_5 \pm 0.2$	$+33 \pm 1$	-6.5 ± 1.4	0.83 ± 0.18	0.65	30
Rh	1.16	4.38	6	-30.5 ± 0.2		-184 ± 2	34.7 ± 0.4	1.64	28
Rh	2.77	11.02	9	-30.43 ± 0.06	-36 ± 1			1.13	25
				$A = -28.5 \pm 2.3$					

† TEF measurement on annealed wire.
‡ Excluded in the determination of A.
§ Measured up to 8 K.

constant ($E_0^{T_b} = \int_0^{T_b} S\,dT$, S being the TEP) while the second term, which concerns electron scattering from spurious magnetic impurities, has the form suggested by Kondo (1965). In our case the main contribution came from iron, which causes negative values of C since the TEP of **Cu**Fe is strongly negative. The value of $T_0 = 3.25$ K is estimated by Pemberton and Guénault (1971) from the data of Gold *et al* (1960) on a dilute **Cu**Fe alloy. A thorough discussion of the reliability of this value of T_0 and the effects of changes in it on the other parameters in the least-squares analysis has been given for homovalent copper alloys by Guénault (1974). The third term in (2) is the sum of two components of the diffusion TEP ($P_1 = A + D$). One component, A, is due to electron scattering from non-magnetic impurities and will be analysed in terms of scattering phase shifts (see § 4). The other component, D, is due to dislocations. By measuring samples in the as-drawn and the annealed state it is possible to deduce A (see, e.g., Julianus *et al* 1984a). Finally, the last term P_3 is a sum of phonon drag, B, and higher-order terms in the electron scattering, A_3. In the as-drawn wires B is supposed to be completely suppressed by the dislocations in the samples (van Baarle *et al* 1967) and thus $P_3 = A_3$.

Concentration-independent values of A are expected for each system. The low-resistance samples were therefore annealed to remove the dislocation contribution, D, to P_1. An unfortunate feature of the present work on copper alloys compared with the work on gold alloys (Julianus *et al* 1984a) and especially silver alloys (Guénault 1967) is that the iron contamination is much more difficult to suppress, making the uncertainty in P_1 and P_3 larger. In alloys where C was large the variation of T_0 resulted in considerable changes in the other parameters. We have restricted ourselves to the value of T_0 mentioned above. The amount of iron in solid solution can be estimated from C using the Nordheim–Gorter rule (see, e.g., Julianus *et al* 1984a)

$$c_{\mathrm{Fe}} = \frac{\Delta\rho}{(\Delta\rho/c)_{\mathbf{CuFe}}} \frac{C}{S_{\mathbf{CuFe}}}. \tag{3}$$

The experimental values are $S_{\mathbf{CuFe}} = -16\,\mu\mathrm{V\,K^{-1}}$ (Blatt *et al* 1976) and $(\Delta\rho/c)_{\mathbf{CuFe}} = 14.5\,\mu\Omega\,\mathrm{cm\,(at.\%)^{-1}}$ (Bass and Fischer 1982). The effect of dissolved iron is most pronounced in the samples with low residual resistance.

From measurements on annealed dilute alloys of gold (Julianus *et al* 1984a) and silver (van Baarle *et al* 1967) it was established that the description of the TEP, $S = P_1 T + P_3 T^3$, was valid only below 4 K. As shown below, the upper limit in annealed copper alloys seems to be at higher temperatures. The results of the least-squares fits to the TEP data are summarised in table 2, in which $\Delta\rho$, as measured on the rod from which the wire was drawn, is also given.

3.2.1. ***Cu****Ni.* The sample with lowest concentration, 1.03 at.% Ni, in the as-drawn form contains a very small amount of iron and the term P_3 is so small that it can be neglected. The measurement on the 2.03 at.% Ni sample can be fitted up to 14 K where the term P_3 is again negligible. The values of P_1 in the as-drawn 1.03 and 2.03 at.% Ni samples do not coincide within the uncertainties. Annealing the 1.03 at.% Ni sample did not bring agreement between these two values. $|P_1|$ in the annealed sample was even smaller than in the as-drawn sample. The fit could be extended only up to 4 K and showed a small positive value of P_3. Earlier measurements by Schroeder *et al* (1965) between 4.2 and 300 K indicated that the addition of 1 at.% Ni to Cu could suppress the phonon drag completely. The resulting value of P_1 from the fit to the 3.02 at.% Ni sample favours the value of P_1 for the 2.03 at.% Ni sample, although this is not completely convincing in view of its large iron content, (22 ± 4) PPM, as determined by atomic absorption techniques, which is rather

higher than estimated from the value of C of the least-squares fit. In summary, the term P_3 in the as-drawn alloys was negligible and the value of A was slightly dependent on concentration. The value for A ((-67.4 ± 1.6) nV K^{-2}) agrees with that obtained in recent measurements by Guénault and Lawson (1981) on annealed 0.5, 1.0 and 2.0 at.% **Cu**Ni samples ($A = (-66 \pm 3)$ nV K^{-2}).

*3.2.2. **Cu**Pd.* In the **Cu**Pd system iron contamination of most of the samples was severe. The Kondo term in (2) contributes more than 50% of the measured TEF at 8 K of the 1.61, 2.47 and 5.18 at.% Pd samples. Therefore the uncertainties in the parameters are large for these three samples. Nevertheless, the values of P_1 and P_3 were consistent, and indicated that P_3 is negative. The 3.42 at.% Pd sample had a very low iron contamination and a more precise establishment of the parameters was possible. The resulting parameters obtained for this sample were consistent with those of the other three samples and, moreover, it was possible to confirm (because of the small error bars) that the coefficient P_3 is negative for the **Cu**Pd system.

*3.2.3. **Cu**Pt.* In this system there were few problems with traces of iron. In the as-drawn 3.09 at.% Pt sample a small term C was observed but in the other as-drawn samples iron contamination was not observed; indeed the fits, including the Kondo term, gave positive values of C and variation of T_0 does not make C negative. All the as-drawn samples

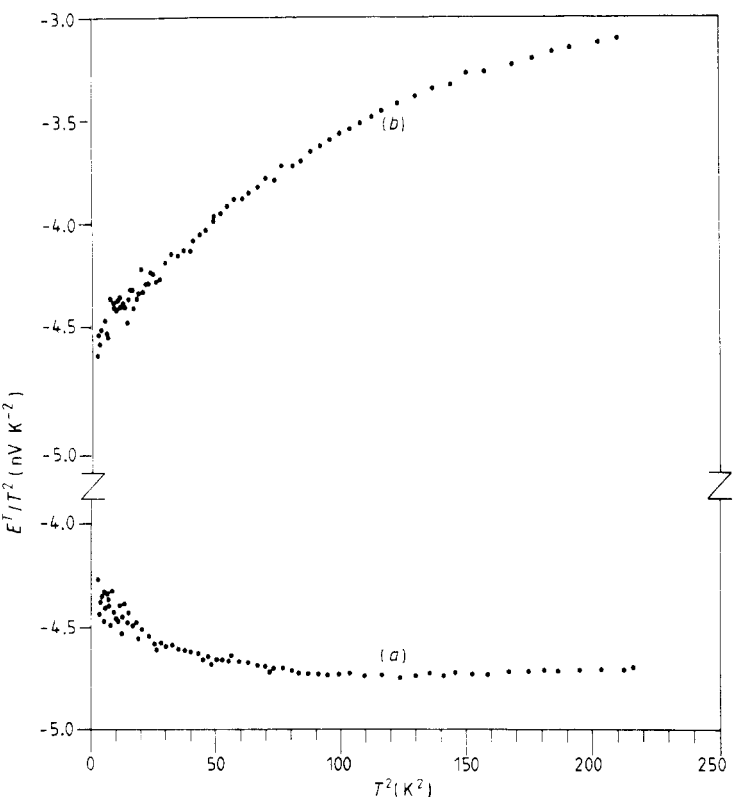

Figure 3. Low-temperature TEF of (*a*) the as-drawn and (*b*) the annealed 0.99 at.% **Cu**Pt sample. The abscissa and slope give $\frac{1}{2}P_1$ and $\frac{1}{4}P_3$, respectively.

showed a small, negative, concentration-independent term P_3 up to 6 K. The uncertainties in the parameters in (2) for the 3.09 at.% Pt sample are large because the parameter C is not small due to the large iron contamination.

For the annealed 0.99 at.% Pt sample a fit imposing the constraint $C=0$ showed that the data could be fitted as high as 8 K. The resulting value of $|P_1|$ was higher than in the as-drawn sample, but still smaller than in the other two samples of higher concentration. Lifting the constraint $C=0$ enlarged the difference. The value of P_3 is found to be small and positive (figure 3) as in **Cu**Ni.

*3.2.4. **Cu**Rh.* The fit for the as-drawn 2.77 at.% Rh sample, including $E_{T_b}^T$, P_1, P_3 and C, resulted in positive values of C indicating that this sample was not noticeably contaminated with iron. A three-parameter fit with the constraint $C=0$ resulted in a negative term P_3 up to 9 K. The four-parameter fit for the as-drawn 1.16 at.% Rh sample gave $P_3=0$ within the uncertainties. Imposing the constraint $P_3=0$ resulted in the same value of P_1 as for the 2.77 at.% Rh sample. The value of C from this fit indicates a severe iron contamination, the iron term contributing approximately one third of the measured TEF at 9 K. The 0.62 at.% Rh sample was measured only after annealing. The analysis of the data for this sample produces a fit with an upper limit of 11 K. The resulting value of $|P_1|$ is much lower than in the other two as-drawn samples of higher concentration. The term C corresponds to a very small iron concentration. If we take $C=0$, systematic deviations occur above about 5 K. The resulting value of P_1 is closer to those of the other Rh samples and P_3 is positive irrespective of the value of C assumed.

3.3. UPS measurements

The spectra are accumulated in energy intervals of 37.5 meV until there are approximately 10^5 counts in the channel recording the highest intensity. In figure 4(*a*) the spectra of Cu and 2.77 at.% **Cu**Rh are shown together with the background contribution to the spectrum (full curve) due to inelastic scattering of the photoelectron. An estimate for this contribution was obtained assuming a step-like energy-loss spectrum (McLachlan *et al* 1975) and by taking the analyser transmission function (Gardner and Samson 1975) into account. After subtracting the energy-loss backgrounds from both the Cu and **Cu**Rh spectra the normalising factor is determined as the quotient of the integrated remaining parts of the spectra. The raw UPS spectra are scaled with these factors and the difference spectrum is calculated. The detailed arguments behind the calculation of the difference spectrum will be presented later (van der Marel *et al* 1985). The result is a change in the density of states weighted with optical matrix elements. A broad d-resonance peak is clearly visible at a binding energy of approximately 1.2 eV. In addition, there are many sharply peaked structures in the region of the host d band. These structures are observed in many other systems and are due to backscattering at the surrounding host potentials. The negative values of the difference spectrum below the bottom of the Cu d band are due to a small decrease of the background contribution to the alloy spectrum relative to the copper spectrum. In a detailed analysis of the UPS spectra that will be given elsewhere (van der Marel *et al* 1985), the positive structure at about 1.2 eV and the sharply peaked structures in the host d-band region are compared with model calculations (Clogston 1961) of the difference spectra including the UPS matrix elements. The model calculations also give the local density of states at the impurity site. In figure 4(*b*) such a function is shown for a Rh impurity in a Cu host. We see that the local density of d states deviates from simple Lorentzian behaviour in the region of high binding energy, but has a more or less pure

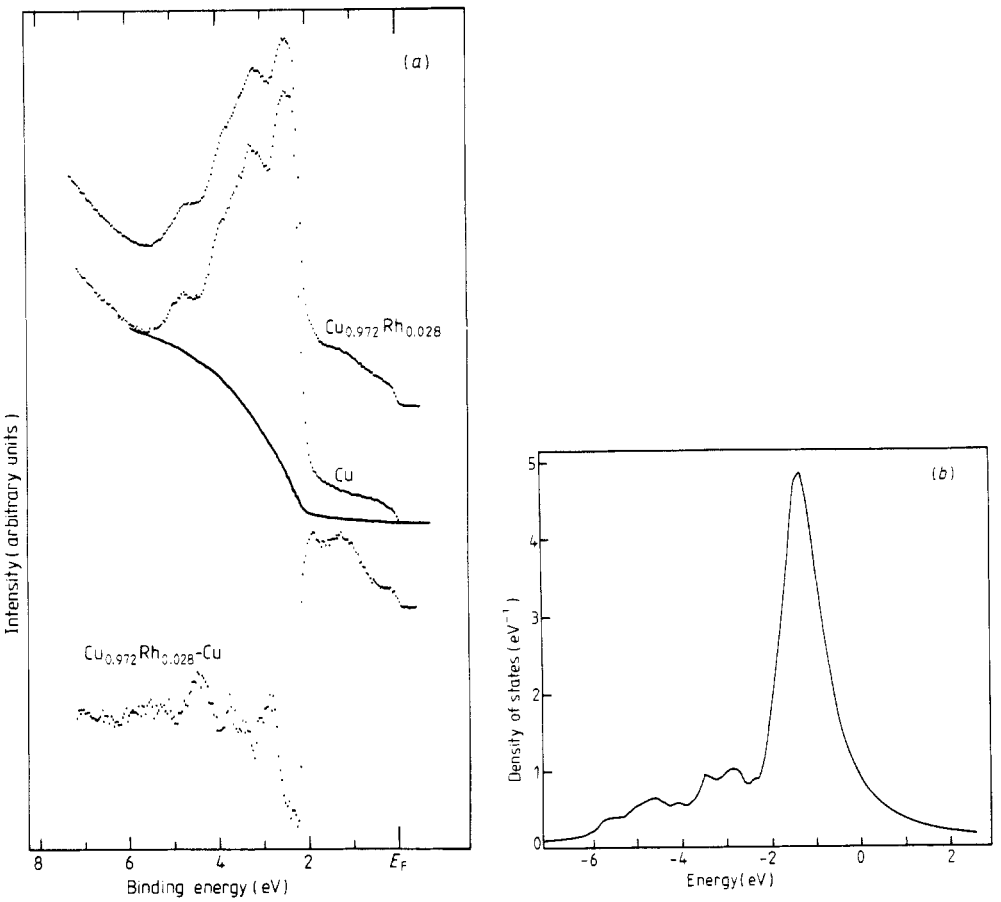

Figure 4. (*a*) UPS ($\hbar\omega = 21.2$ eV) spectra of Cu, 2.8 at.% **Cu**Rh and the difference spectrum. (*b*) The calculated local density of d states at a Rh impurity embedded in a Cu host.

Lorentzian lineshape in the region of ε_F. The local impurity d density of states can be integrated up to ε_F to provide the partial screening charge Z_2. These values, together with the density of states at ε_F and the peak maxima, are given in table 3.

Table 3. Resonant d-state parameters from UPS measurements.

Alloy	E_d (eV)	$n_d(\varepsilon_F)$ (eV^{-1})	Z_2
CuNi[a]	−0.78	1.48	−1.2†
CuPd[b]	−1.8 ± 0.1	0.24	−0.4 ± 0.05
CuPt[b]	−1.8 ± 0.1	0.32	−0.5 ± 0.05
CuRh[c]	−1.15 ± 0.1	0.95	−1.4 ± 0.05

[a] Bosch (1982); [b] van der Marel *et al* (1985); [c] this work.
† **Cu**Ni is probably a highly correlated system needing a more careful analysis than the other alloys.

4. Analysis of transport and UPS data

In noble-metal hosts the d states of the solute hybridise with the conduction band of the host leading to resonant d states. The alloy can be represented within the GB model by sets of s, p and d phase shifts (φ_l^{GB}, $l=0, 1, 2$). In this section we shall work only in the GB model and the superscript will be omitted. We present two different methods of deriving the sets of φ_l from the experimental data. In the first method phase shifts are derived from the Friedel sum rule, the experimental residual resistivity and the TEP using the position of the resonant d state as obtained from the peak in the UPS and assuming a Lorentzian lineshape. Alternatively, the phase shifts φ_l can be obtained from the Friedel sum, the resistivity and φ_2 as obtained from the UPS. The second method of analysis is perhaps more satisfactory because it does not involve the assumption of a Lorentzian lineshape. We will start with a general framework which is common to both methods.

The Friedel sum, $\tilde{F}$, can be written in terms of φ_0, φ_1 and φ_2 as

$$\tilde{F}=2\pi^{-1}\varphi_0(\varepsilon_F)+6\pi^{-1}\varphi_1(\varepsilon_F)+10\pi^{-1}\varphi_2(\varepsilon_F). \tag{4}$$

In the absence of local lattice distortion and charge transfer between the impurity and the nearest-neighbour host atoms the Friedel sum $\tilde{F}$ is just the valence difference between solute and solvent, ΔZ. A phenomenological correction for local lattice distortion by Blatt (1957) leads to a modified Friedel sum $\tilde{F}_{\text{Blatt}}=\Delta Z-(3/\gamma_E)\delta a/a$ where $\gamma_E=3(1-\sigma)/(1+\sigma)$ ($=1.45$ for a copper host), σ being the Poisson ratio and $\delta a/a$ the relative change in the lattice parameter per at.% solute as deduced from Pearson (1958). A correction for charge transfer could also be made by modification of the Friedel sum.

The residual resistivity in the GB model is†

$$\frac{\Delta\rho}{c}=\frac{3\pi\hbar V}{(\pi e\hbar v_F N(\varepsilon_F))^2}\rho^0(\varepsilon_F) \tag{5a}$$

where

$$\rho^0(\varepsilon)=\sum_{l=0}^{2}(l+1)\sin^2(\varphi_l(\varepsilon)-\varphi_{l+1}(\varepsilon)). \tag{5b}$$

Here $N(\varepsilon)$ is the density of states of one spin direction and V is the volume of the unit cell. The prefactor in (5*a*) reduces to $3\pi^3\hbar^5/Ve^2m^2\varepsilon_F^2$ in the free-electron case and has a numerical value of 3.8 $\mu\Omega$ cm (at.%)$^{-1}$ for copper-based alloys.

The coefficient of the linear component of the diffusion TEP, A, (see § 3.2) depends on both the phase shifts and the derivatives of the phase shifts with respect to the energy at ε_F. The strong energy dependence of the resonant d phase shift makes it possible to reduce the number of variables by assuming that the energy dependence of the s and p phase shifts is negligible, i.e.

$$(\partial\varphi_l/\partial\varepsilon)|_{\varepsilon=\varepsilon_F}=0 \qquad \text{for } l=0, 1. \tag{6}$$

The expression for A is then given by (see, e.g., Julianus *et al* 1984b)

$$A=\frac{\pi^2k_B^2}{3|e|}\left(\frac{2}{\varepsilon}+\frac{A^0(\varepsilon)}{\rho^0(\varepsilon)}\right)\Bigg|_{\varepsilon=\varepsilon_F} \tag{7a}$$

† The same formula was derived by Schöpke and Mrosan (1978).

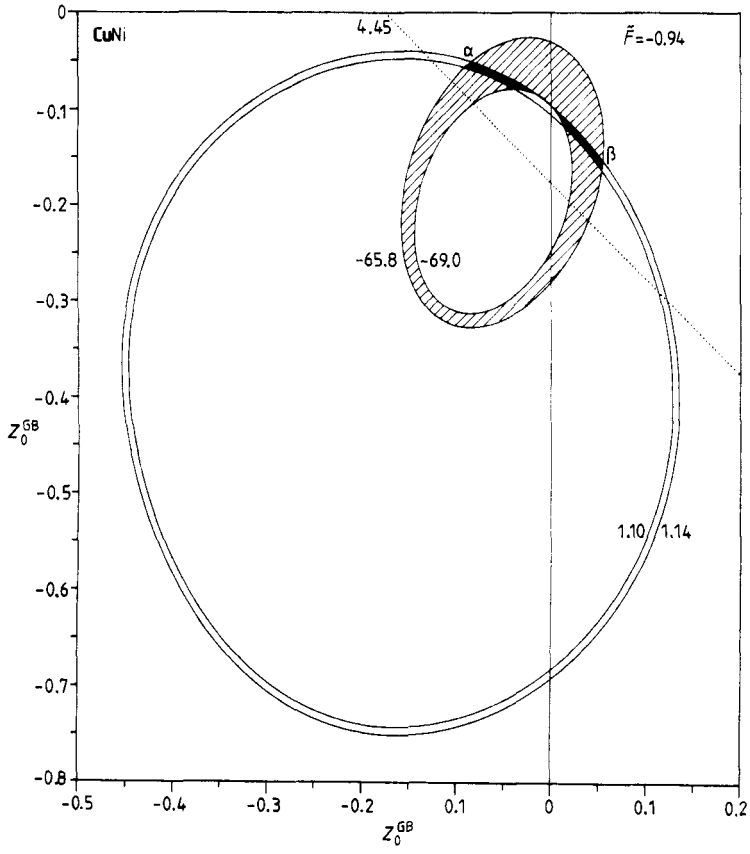

Figure 5. **Cu**Ni: computed loci of constant values of $\Delta\rho/c$ (band between full curves), A (shaded band) and $(1/c)\Delta\gamma/\gamma$ (dotted) in the GB model for $\tilde{F}=\tilde{F}_{\text{Blatt}}=-0.94$. The curves for A and $(1/c)\Delta\gamma/\gamma$ are for $E_d=-0.78$ eV.

where

$$A^0(\varepsilon)=(3\sin 2\varphi_2(\varepsilon)-2\sin 2(\varphi_1(\varepsilon)-\varphi_2(\varepsilon)))\hat{c}\varphi_2(\varepsilon)/\hat{c}\varepsilon. \tag{7b}$$

The first term in A is -6.9 nV K^{-2} for copper-based systems. Strictly speaking, this factor should be modified slightly due to the different prefactor for $\Delta\rho/c$ in (5*a*) compared with the free-electron value. The modification will mainly affect our conclusions regarding the systems **Cu**Pd and **Cu**Pt, where the experimental value of A is close to the first term on the right-hand side of (7*a*). Moreover, in these systems the top of the peak due to the resonant d state is far from the Fermi energy, and the neglect of the energy dependence of the s and p phase shifts could be questionable.

In the case of **Cu**Ni there is additional information from the specific heat data of Guthrie *et al* (1959). The relative change in the electronic specific heat coefficient, γ, can be expressed as (Daniel and Friedel 1965)

$$\frac{1}{c}\frac{\Delta\gamma}{\gamma}=\frac{10\varepsilon}{3\pi}\frac{\hat{c}\varphi_2(\varepsilon)}{\hat{c}\varepsilon}\bigg|_{\varepsilon=\varepsilon_F}. \tag{8}$$

It is convenient to work with partial screening charges defined as

$$Z_l = \frac{2(2l+1)}{\pi}\varphi_l, \tag{9}$$

the use of these quantities in contour plots of Z_1 against Z_0 having been described by Julianus *et al* (1984b). In brief, the residual resistivity is determined at every point of the Z_0, Z_1 plot after specifying the Friedel sum (cf equations (4), (5) and (9)). The same holds for A when the derivative of the d phase shift is known at ε_F. The points in the Z_0, Z_1 plot which represent the experimental values (cf tables 1 and 2) form the contours seen, for example, in figure 5, the contours being broadened to bands due to the experimental uncertainties. The intersections of the bands for $\Delta\rho/c$ and A (see § 4.1) or $\Delta\rho/c$ and Z_2 (see § 4.2) in the Z_0, Z_1 plots give sets of phase shifts which represent both experimental quantities. Again due to the experimental uncertainties, the sets of solutions form ranges of acceptable phase shifts.

4.1. First method of analysis

The assumed Lorentzian lineshape employed in the first method of analysis corresponds to an energy dependence of the d phase shift given by

$$\tan\varphi_2(\varepsilon) = \frac{\frac{1}{2}\Gamma}{E_d - (\varepsilon - \varepsilon_F)} \tag{10}$$

where E_d and Γ are the position, relative to the Fermi energy ε_F, and the full width at half maximum (FWHM) of the resonant d state, respectively (see figure 1). The extra local density of d states $n_d(\varepsilon)$ associated with the d-resonance peak is directly related to the derivative of the d phase shift by

$$n_d(\varepsilon) = \frac{10}{\pi}\frac{\partial\varphi_2(\varepsilon)}{\partial\varepsilon} \tag{11a}$$

or using the Lorentzian lineshape as

$$n_d(\varepsilon) = \frac{10}{\pi}\frac{\frac{1}{2}\Gamma}{E_d^2 + (\frac{1}{2}\Gamma)^2}. \tag{11b}$$

The expressions (7*b*) for $A^0(\varepsilon_F)$ and (8) for $(1/c)\Delta\gamma/\gamma$ can be written, using (10), as

$$A^0(\varepsilon_F) = (3\sin 2\varphi_2(\varepsilon_F) - 2\sin 2(\varphi_1(\varepsilon_F) - \varphi_2(\varepsilon_F)))\frac{1}{2E_d}\sin 2\varphi_2(\varepsilon_F) \tag{12}$$

and

$$\frac{1}{c}\frac{\Delta\gamma}{\gamma} = \frac{10}{3\pi}\frac{\varepsilon_F}{E_d}\sin 2\varphi_2(\varepsilon_F). \tag{13}$$

The prefactor in (13) is $7.5/E_d$ for copper-based systems.

We have considered two values of the Friedel sum, $\tilde{F}_{\text{Blatt}}$ and ΔZ. For each system we have given a Z_0, Z_1 plot (figures 5–8) using $\tilde{F}_{\text{Blatt}}$ and the influence of different Friedel sums is illustrated in table 4(*a*) for $\tilde{F}$ equal to $\tilde{F}_{\text{Blatt}}$ and ΔZ. The plots for **Cu**Ni, **Cu**Pd and **Cu**Pt (figures 5–7) contain the band representing A using the central value of E_d from the UPS measurements (table 3). The plot for **Cu**Rh shows two bands for A corresponding to

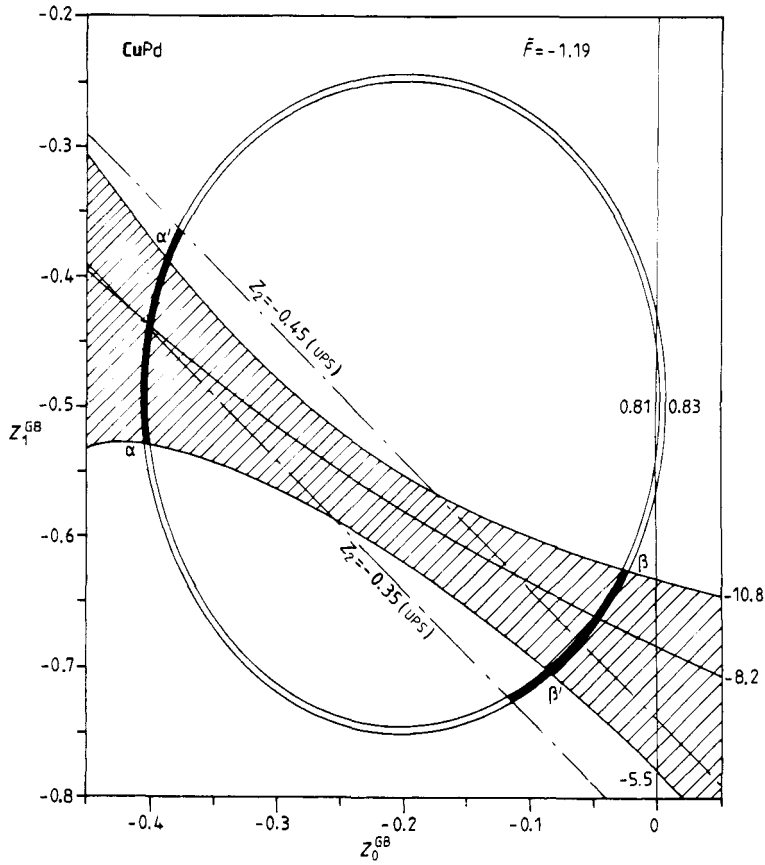

Figure 6. **Cu**Pd: computed loci of constant values of $\Delta\rho/c$ (band between full curves) and A (shaded band) in the GB model for $\tilde{F}=\tilde{F}_{\text{Blatt}}=-1.19$. The band for A is for the central value of E_d (table 3).

the extreme values in table 3. In all plots we find two possible solution ranges for the phase shifts, α and β, fulfilling the Friedel sum and describing the experimental quantities $\Delta\rho/c$ and A, etc, within the GB model.

For **Cu**Pd and **Cu**Pt the solutions for Z_0 and Z_1 are quite insensitive to changes in E_d because the experimental values for A are close to the value of the first term in (7*a*). For these systems there are even Z_l solutions for values of E_d less than -4 eV, which would mean that the resonant d state was lying deep in the copper d band. In the other two systems, **Cu**Ni and **Cu**Rh, the bands for A are very sensitive to changes in E_d. For instance, in the case of **Cu**Ni solutions exist for $E_d=-0.78$ eV and $\tilde{F}=-0.94$, but for $E_d=-0.83$ eV and the same value of $\tilde{F}$ no set of phase shifts is able to describe both $\Delta\rho/c$ and the TEP.

In the cases of **Cu**Ni, **Cu**Pd and **Cu**Pt the solution ranges for Z_l are small because of the closed contours in the Z_0, Z_1 plots which follow from their low resistivity. The A bands for **Cu**Pd and **Cu**Pt extend over a wide range of Z_0 values and are only slightly modified by assuming an energy dependence of the s and p phase shifts. The modification is even smaller, as expected from the higher $|A|$ value, in the cases of **Cu**Ni and **Cu**Rh. Therefore we conclude that our assumption that the derivatives of the s and p phase shifts with respect to energy at the Fermi level are equal to zero has only a minor influence on the

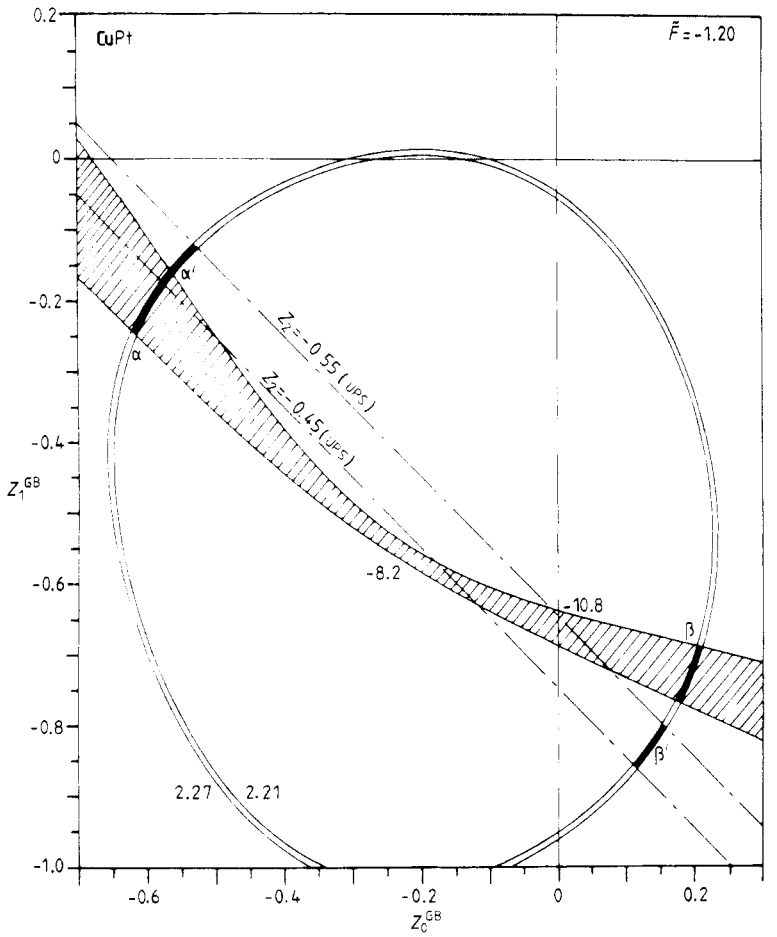

Figure 7. CuPt: computed loci of constant values of $\Delta\rho/c$ (band between full curves) and A (shaded band) in the GB model for $\tilde{F}=\tilde{F}_{\text{Blatt}}=-1.20$. The band for A is for the central value of E_d (table 3).

solution ranges Z_l. Solution type α has a more negative Z_0 contribution and less negative Z_1 and Z_2 contributions than type β. The latter fact means that the number of d electrons taking part in the screening of the solute is largest for solution type α.

The values of Γ for the Z_l solution ranges α and β are calculated from Z_2 using (10) and subsequently $n_d(\varepsilon_F)$ is obtained using (11*b*). The $n_d(\varepsilon_F)$ and Z_2 values in table 4(*a*) show, with the exception of **Cu**Ni, good agreement with the UPS measurements (table 3), which is surprising in view of the complexity of the UPS difference spectra and apparent deviation from Lorentzian lineshape. This means that, although the Lorentzian shape for the d-resonance peak is an oversimplification (figure 1), together with the experimental $\Delta\rho/c$ and A values it gives the correct density of d states at ε_F and the right amount of d screening charge. This is probably because the lineshape is noticeably non-Lorentzian only at energies well below ε_F.

In figure 5 the curve representing the experimental change in the electronic specific heat coefficient, computed with (13), is included. The value $E_d=-0.78$ eV gives two small solution ranges to $\Delta\rho/c$ and A in the Z_0, Z_1 plot which, moreover, also satisfy $(1/c)\Delta\gamma/\gamma$ when the experimental uncertainties in this quantity are included, though these were

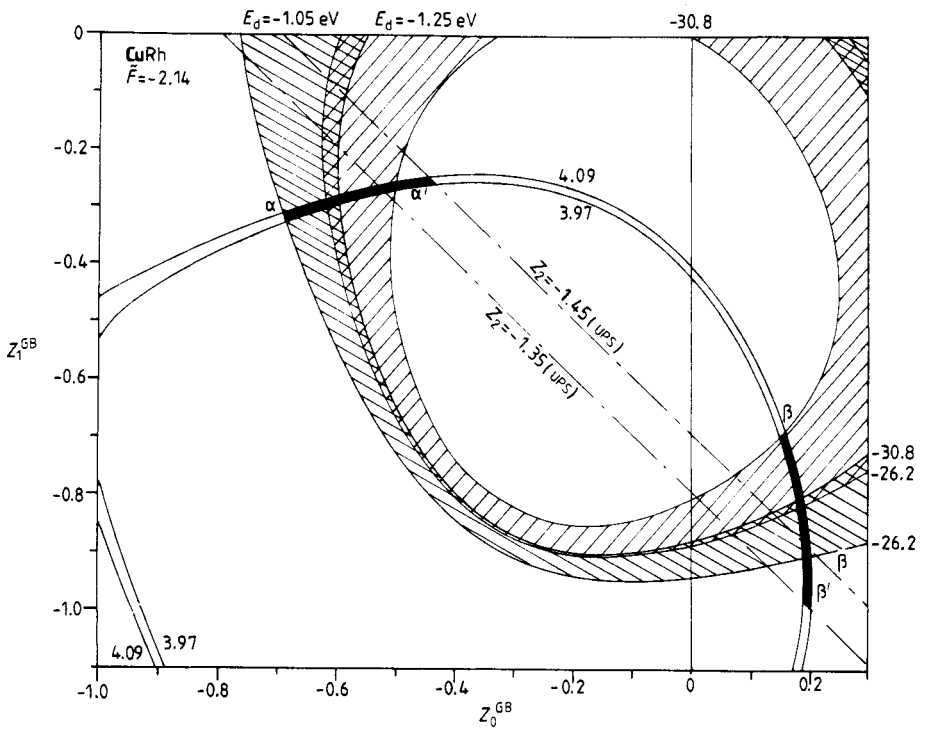

Figure 8. **Cu**Rh: computed loci of constant values of $\Delta\rho/c$ (band between full curves) and A (shaded bands) in the GB model for $\bar{F} = \bar{F}_{\text{Blatt}} = -2.14$. The two bands for A correspond to the uncertainty in E_d (table 3).

difficult to estimate from the original measurements. The $(1/c)\Delta\gamma/\gamma$ values corresponding to sets α and β in figure 5 are 4.69 ± 0.05 and 4.84, respectively, to be compared with the experimental value of 4.45 (Guthrie *et al* 1959).

4.2. Second method of analysis

In this method Z_2 is taken from the UPS data and is included in the usual Z_0, Z_1 plot to give a straight line at $-45°$, drawn (cf equation (4)) for a given Friedel sum. The partial screening charges Z_0 and Z_1 are then determined by the intersection of the band representing Z_2 with the band representing $\Delta\rho/c$ on the Z_0, Z_1 plot (figures 5–8). In the plots for **Cu**Pd, **Cu**Pt and **Cu**Rh again two solution ranges, α' and β', are found which are in good agreement with the Z_l solutions obtained in the previous section where the assumption of a Lorentzian lineshape of the d-resonance peak was made. There is some evidence from UPS measurements (Bosch *et al* 1984) and optical absorption measurements (Beaglehole 1976) that **Cu**Ni is a highly correlated system or that spin fluctuations are important. Therefore it is interesting to note that solutions compatible with $\Delta\rho/c$ should be in the range $-0.85 < Z_2 < 0$ but that the value of Z_2 from the UPS data is -1.2, leading to no solutions.

In the cases of **Cu**Pd, **Cu**Pt and **Cu**Rh the linear term in the TEP, A, was calculated for the Z_l solution ranges α' and β' in figures 6–8 with equations (7) and (11*a*), using the derivative of the d phase shift obtained from $n_d(\varepsilon_F)$ of the UPS (table 4(*b*)). There is good agreement with the experimental values of A in table 2.

Table 4. (*a*) Partial screening charges in the GB model satisfying the Friedel sum ($\tilde{F}=\Delta Z^{a}$ or $\tilde{F}=\tilde{F}_{\text{Blatt}}{}^{b}$) and accounting for $\Delta\rho/c$ and A (see § 4.1). The two sets of partial screening charges are labelled α and β (see figures 5–8).

	Input		Output				
Alloy	$\tilde{F}$	E_d (eV)	Set	Z_0^{GB}	Z_1^{GB}	Z_2^{GB}	$n_d(\varepsilon_F)$ (eV^{-1})
CuNi	-1.00^{a}	-0.78	α	$-0.11\rightarrow-0.07$	$-0.10\rightarrow-0.08$	$-0.83\rightarrow-0.81$	$0.99\rightarrow1.02$
			β	$+0.02\rightarrow0.05$	$-0.20\rightarrow-0.16$	$-0.86\rightarrow-0.85$	$1.04\rightarrow1.05$
	-0.94^{b}	-0.78	α	$-0.09\rightarrow-0.04$	$-0.08\rightarrow-0.05$	$-0.82\rightarrow-0.80$	$0.98\rightarrow1.00$
			β	$+0.01\rightarrow0.05$	$-0.16\rightarrow-0.11$	-0.84	1.02
CuPd	-1.00^{a}	-1.80	α	$-0.40\rightarrow-0.36$	$-0.48\rightarrow-0.27$	$-0.37\rightarrow-0.13$	$0.07\rightarrow0.22$
			β	$-0.02\rightarrow+0.04$	$-0.63\rightarrow-0.54$	$-0.50\rightarrow-0.34$	$0.20\rightarrow0.29$
	-1.19^{b}	-1.80	α	$-0.41\rightarrow-0.38$	$-0.53\rightarrow-0.38$	$-0.42\rightarrow-0.25$	$0.15\rightarrow0.24$
			β	$-0.09\rightarrow-0.02$	$-0.70\rightarrow-0.62$	$-0.55\rightarrow-0.40$	$0.23\rightarrow0.31$
CuPt	-1.00^{a}	-1.80	α	$-0.59\rightarrow-0.52$	$-0.14\rightarrow-0.04$	$-0.44\rightarrow-0.27$	$0.15\rightarrow0.24$
			β	$+0.23\rightarrow0.27$	$-0.68\rightarrow-0.59$	$-0.67\rightarrow-0.55$	$0.30\rightarrow0.36$
	-1.20^{b}	-1.80	α	$-0.63\rightarrow-0.56$	$-0.23\rightarrow-0.15$	$-0.47\rightarrow-0.37$	$0.19\rightarrow0.27$
			β	$+0.17\rightarrow0.21$	$-0.78\rightarrow-0.68$	$-0.73\rightarrow-0.59$	$0.32\rightarrow0.39$
CuRh	-2.00^{a}	-1.15	α	$-0.63\rightarrow-0.52$	$-0.23\rightarrow-0.19$	$-1.28\rightarrow-1.15$	$0.91\rightarrow1.00$
			β	$+0.20\rightarrow0.24$	$-0.80\rightarrow-0.68$	$-1.42\rightarrow-1.53$	$1.08\rightarrow1.14$
	-2.14^{b}	-1.15	α	$-0.66\rightarrow-0.55$	$-0.31\rightarrow-0.26$	$-1.33\rightarrow-1.17$	$0.92\rightarrow1.03$
			β	$+0.16\rightarrow0.20$	$-0.86\rightarrow-0.74$	$-1.58\rightarrow-1.46$	$1.10\rightarrow1.16$

Table 4. (*b*) Partial screening charges in the GB model satisfying the Friedel sum ($\tilde{F}=\tilde{F}_{\text{Blatt}}$) and accounting for $\Delta\rho/c$ and $n_d(\varepsilon_F)$ and Z_2 from UPS (see § 4.2). The two sets of partial screening charges are labelled α' and β' (see figures 5–8).

	Input			Output			
Alloy	$\tilde{F}$	$n_d(\varepsilon_F)$ (eV^{-1})	Z_2	Set	Z_0^{GB}	Z_1^{GB}	A ($nV\,K^{-2}$)
CuNi	-0.94	1.48	-1.2			No solution	
CuPd	-1.19	0.24	$-0.45\rightarrow-0.35$	α'	$-0.41\rightarrow-0.37$	$-0.44\rightarrow-0.36$	$-12.3\rightarrow-8.4$
				β'	$-0.12\rightarrow-0.06$	$-0.73\rightarrow-0.68$	$-7.0\rightarrow-3.7$
CuPt	-1.20	0.32	$-0.55\rightarrow-0.45$	α'	$-0.58\rightarrow-0.52$	$-0.19\rightarrow-0.12$	$-13.0\rightarrow-11.1$
				β'	$0.11\rightarrow0.16$	$-0.86\rightarrow-0.80$	$-7.1\rightarrow-5.5$
CuRh	-2.14	0.95	$-1.45\rightarrow-1.35$	α'	$-0.52\rightarrow-0.42$	$-0.28\rightarrow-0.25$	$-32.3\rightarrow-29.7$
				β'	$0.18\rightarrow0.20$	$-0.99\rightarrow-0.88$	$-23.2\rightarrow-19.6$

The weakness of the first method of analysis lies in the assumption of a Lorentzian lineshape for the resonant d-state peak in the local density of states in the UPS. The weakness of the second method is probably in the assumption that the local density of states deduced from the UPS is d like only. The overall agreement between the results of both methods is reassuring and therefore the Z_l solutions obtained by the first method will be compared in § 6 with the Z_l solutions obtained from DHVA data in the next section.

5. Analysis of DHVA data

$\Delta\rho/c$ and the TEP are averages over the Fermi surface and they give no details on the Fermi surface anisotropy or on the electron scattering anisotropy. A technique which can probe the anisotropy of conduction-electron scattering over the Fermi surface is the measurement of de Haas–van Alphen (DHVA) oscillations. In addition, independent estimates of the Friedel phase shifts φ_l^{CHL} can be made through the DHVA measurements and these can be compared with φ_l^{GB}. In the following the superscripts GB and CHL will be added only when it is necessary for the sake of clarity.

The Fermi surface changes and electron–impurity scattering can be studied for extremal orbits. The change in the cross-sectional area of an extremal orbit is given by the frequency shift of the DHVA signal and the average scattering rate for an orbit can be represented by the Dingle temperature. A model within the muffin-tin approximation for host and impurity potentials based on a partial-wave analysis has been developed by CHL. In this, phase-shift expressions are derived for frequency changes ΔF,

$$\frac{1}{c}\frac{\Delta F(\omega)}{F_{\mathrm{s}}}=\sum_l\left(\frac{\partial\tilde{A}(\omega)}{\partial\eta_l^{\mathrm{h}}(\varepsilon)}\right)_{\varepsilon=\varepsilon_{\mathrm{F}}}\frac{1}{I_l}\sin\varphi_l\cos\varphi_l, \tag{14}$$

and Dingle temperatures X,

$$\frac{m^*(\omega)X(\omega)}{c}=\frac{\hbar^2}{200\pi^2k_{\mathrm{B}}m_0}\tilde{A}_{\mathrm{FE}}\sum_l\left|\left(\frac{\partial\tilde{A}(\omega)}{\partial\eta_l^{\mathrm{h}}(\varepsilon)}\right)_{\varepsilon=\varepsilon_{\mathrm{F}}}\right|\frac{1}{I_l}\sin^2\varphi_l. \tag{15}$$

Equations (14) and (15) are in units of the free-electron-sphere cross section ($\tilde{A}_{\mathrm{FE}}$) per unit concentration and K (at.%)$^{-1}$, respectively, and $F_{\mathrm{s}}=(\hbar/2\pi e)\tilde{A}_{\mathrm{FE}}$. The wavefunction coefficients $(\partial\tilde{A}(\omega)/\partial\eta_l^{\mathrm{h}}(\varepsilon))_{\varepsilon=\varepsilon_{\mathrm{F}}}$ and normalisation integrals I_l are tabulated for noble-metal hosts (see CHL). The label ω denotes a specific orbit and $m^*(\omega)$ are the cyclotron masses (we used the experimental values of Lengeler *et al* (1977)). The phase shifts used in Coleridge's model, φ_l, like those used in the GB model, are effective phase shifts. In both models host (η_l^{h}), impurity (η_l^{i}) and backscattering (θ_l) phase shifts are involved, i.e. $\varphi_l=\eta_l^{\mathrm{i}}-\eta_l^{\mathrm{h}}+\theta_l$.

The frequency changes and Dingle temperatures of **CuPd**, **CuPt** and **CuRh** have been measured by CTT. For **CuNi** Poulsen *et al* (1974) and Templeton and Coleridge (1975) measured the Dingle temperatures and frequency shifts, respectively. In their analysis of the DHVA measurements CTT used resistivity values for **CuPd**, **CuPt** and **CuRh** to determine the concentrations of their samples, which differ from those reported here. There is some support from other investigations for the values of $\Delta\rho/c$ reported here and for **CuRh** the difference in the resistivity is considerable, as seen in table 1. The DHVA results have therefore been re-analysed using these new values. The frequency change and Dingle temperature measurements are on five extremal orbits: B_{111}, B_{100}, N_{111}, R_{100} and D_{110}. (The notation for the orbits is B(belly), N(neck), R(rosette) and D(dogsbone).) To obtain a unique set of phase shifts from, for example, the Dingle temperatures, an overcomplete set of equations (15) has to be solved. CTT used a least-squares fitting procedure to the experimental data (m^*X) to do this. The resistivity is used in their case to determine the sign of the phase shifts and the Friedel sum is then obtained as an output parameter. A different approach using Z_0, Z_1 plots was used in the present work. The Friedel sum is an input parameter and fixes Z_2 at every point of the Z_0, Z_1 plot. Consequently, the contours on the Z_0, Z_1 plot representing the Dingle temperatures can be calculated from (15). The contours are broadened as before to bands allowing for the experimental uncertainties. For

Table 5. Range of $\tilde{F}$ for [a] X, [b] X and $\Delta\rho/c$ and [c] ΔF in the CHL model. The indices (α'') and (β'') refer to different types of solutions (see text).

Alloy	$\tilde{F}_{\text{Blatt}}$	$\tilde{F}$ [a]	[b]	[c]	ΔZ
CuNi	−0.94	−0.88 → −0.69	−0.80 → −0.71	—	−1
CuPd	−1.19	−1.20 → −0.80(α'') −1.20 → −0.20(β'')	−1.20 → −1.14(α'') −1.20 → −1.14(β'')	−1.9 → −0.97	−1
CuPt	−1.20	−1.10 → −0.06(β'') −1.53 → 0 (α'')	−1.08 → −0.90(β'') −0.36 → −0.21(α'')	−1.94 → −0.91	−1
CuRh	−2.14	−2.10 → −1.0	−1.99 → −1.00	−2.68 → −1.41	−2

a solution to exist, the bands of all five orbits must have a common region of intersection. The same approach is followed for the frequency shifts.

In the Z_0, Z_1 plots for Dingle temperatures the experimental residual resistivity, now calculated within the CHL model, is also included. For Dingle temperatures local lattice distortion again leads to the Friedel sum $\tilde{F}_{\text{Blatt}}$. For the frequency shifts, however, the effects of long-range lattice distortion can be allowed for simply by taking into account the effects of the lattice parameter changes with alloying on the experimental frequency shifts themselves (see CTT). The frequency shifts are likely to be insensitive to local lattice distortion because the effect on the anisotropy of the Fermi surface is small (Lee *et al* 1976).

The Blatt correction to the Friedel sum is an approximation and thus $\tilde{F}_{\text{Blatt}}$ cannot be determined precisely. Friedel sums different from but close to $\tilde{F}_{\text{Blatt}}$ have therefore also been examined. The correction to the experimental frequency shifts can also be made approximately and again Friedel sums slightly different from ΔZ were examined. The ranges of Friedel sums over which solutions exist are listed in table 5, which also contains solutions satisfying both the Dingle temperature and the residual resistivity. Both are scattering properties which are sensitive to local distortions and the constraint of the

Table 6. Sets of Z_l from [a] X, [b] X and $\Delta\rho/c$ and [c] ΔF. Solutions [a] and [b] are those closest to or equal to $\tilde{F}_{\text{Blatt}}$ while solutions [c] are those equal to $\tilde{F} = \Delta Z$. See table 5 for the indices α'' and β''.

Alloy	$\tilde{F}$	Z_0^{CHL}	Z_1^{CHL}	Z_2^{CHL}	$(\Delta\rho/c)_{\text{CHL}}$ ($\mu\Omega$ cm (at.%)$^{-1}$)
CuNi	−0.88[a]	+0.10	−0.24	−0.74	1.01 → 1.05
	−0.80[b]	+0.14 → +0.15	−0.27 → −0.22	−0.72 → −0.67	1.10 → 1.11
CuPd	−1.19[a]	−0.22 → −0.13	−0.37 → −0.30	−0.75 → −0.60	0.72 → 0.83
	−1.19[b]	−0.18 → −0.13	−0.33 → −0.30	−0.75 → −0.69	0.81 → 0.83
	−1.00[c]	−0.27 → +0.17$_5$	−0.39 → +0.21	−0.94$_5$ → −0.40	0.45 → 1.45
CuPt	−1.20[a](α'')	−0.44 → −0.42$_5$	−0.49 → −0.47	−0.29 → −0.27$_5$	1.30 → 1.35
	−1.08[b](β'')	+0.22	−0.29$_5$ → −0.28$_5$	−1.01$_5$ → −1.00$_5$	2.21 → 2.22
	−1.00[c]	−0.36 → −0.33	−0.33$_5$ → −0.28	−0.38 → −0.32	0.81 → 0.93
CuRh	−2.09[a]	−0.38 → −0.27	−0.49 → −0.39	−1.43 → −1.22	2.67 → 3.01
	−1.98[b]	−0.34 → −0.20	−0.20 → −0.17$_5$	−1.58 → −1.46	3.97 → 4.03
	−2.00[c]	−0.80 → −0.76	−0.47 → −0.23	−1.01 → −0.76	3.40 → 4.15

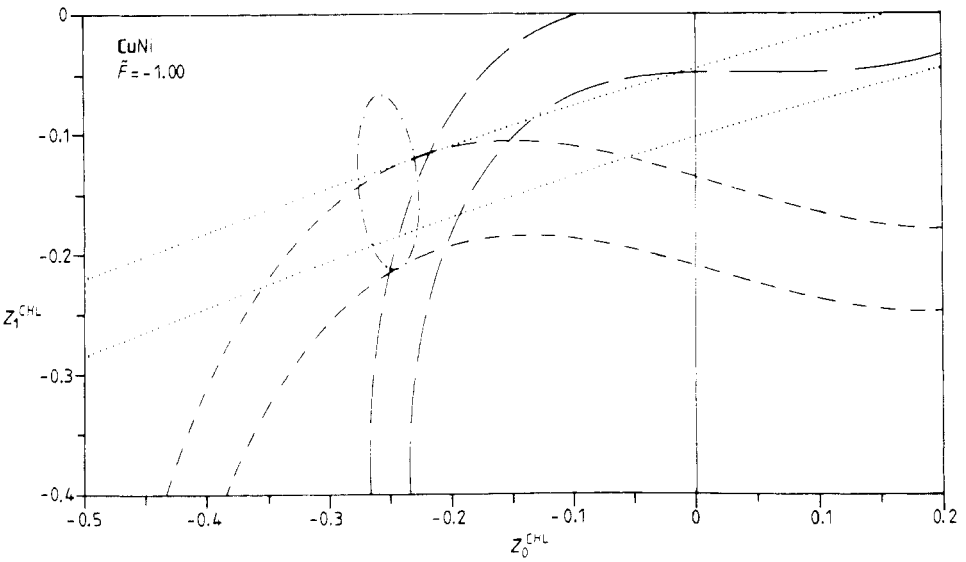

Figure 9. **Cu**Ni: computed loci of constant values of ΔF in the CHL model for $\tilde{F} = \Delta Z = -1.00$. The orbits are B_{100} (– · – · –), N_{111} (· · ·), R_{100} (— —) and D_{110} (– – –).

residual resisitivity reduces the ranges for $\tilde{F}$ dramatically. Certain solution ranges for Z_l deduced from Z_0, Z_1 plots are given in table 6, mainly for $\tilde{F}_{\text{Blatt}}$ and ΔZ.

The graphical procedure followed here probably imposes more stringent requirments on the parameters derived than the techniques followed previously by CHL, Coleridge (1975) and CTT. The Z_l values now obtained differ from those obtained by CTT partly because of this and partly because of the different residual resistivities used in the present work.

5.1. CuNi

CHL deduced a set of phase shifts from the Dingle temperatures, $Z_0 = -0.04$, $Z_1 = -0.08$ and $Z_2 = -0.82$ resulting in a Friedel sum of -0.94, exactly equal to $\tilde{F}_{\text{Blatt}}$. From the Z_0, Z_1 plot using this value of the Friedel sum the R_{100} orbit did not lie in the common region of intersection of the other orbits within the experimental uncertainties. On the other hand, it was also clear that the above set of phase shifts was probably the 'best' one for this Friedel sum. It is found that for $-0.88 < \tilde{F} < -0.69$ (table 5) there are solutions involving all orbits. Moreover, in the range $-0.80 < \tilde{F} < -0.71$ (table 5) a set of Z_l values can be obtained which in addition gives agreement with the experimental value of $\Delta\rho/c$ as calculated using the procedure proposed by CHL. These Z_l values are given in table 6 for $\tilde{F} = -0.80$ where the difference compared with those reported by CHL is entirely due to the different value of $\tilde{F}$ and the difference in analysis, because the same resistivity values were used.

For the frequency changes, Coleridge (1975) obtained $Z_0 = -0.17 \pm 0.1$, $Z_1 = -0.10 \pm 0.08$ and $Z_2 = -0.76 \pm 0.2$, resulting in a Friedel sum of -1.03 ± 0.1. Our plots show that for $\tilde{F} = -1$ (figure 9) a region of common intersection of four bands exists (the B_{111} orbit did not go through this region). In fact there are no values of $\tilde{F}$ which give a solution for all orbits within the uncertainties of the original data. The closest approach to a solution is probably for $\tilde{F} = -1.03$ as found by Coleridge (1975).

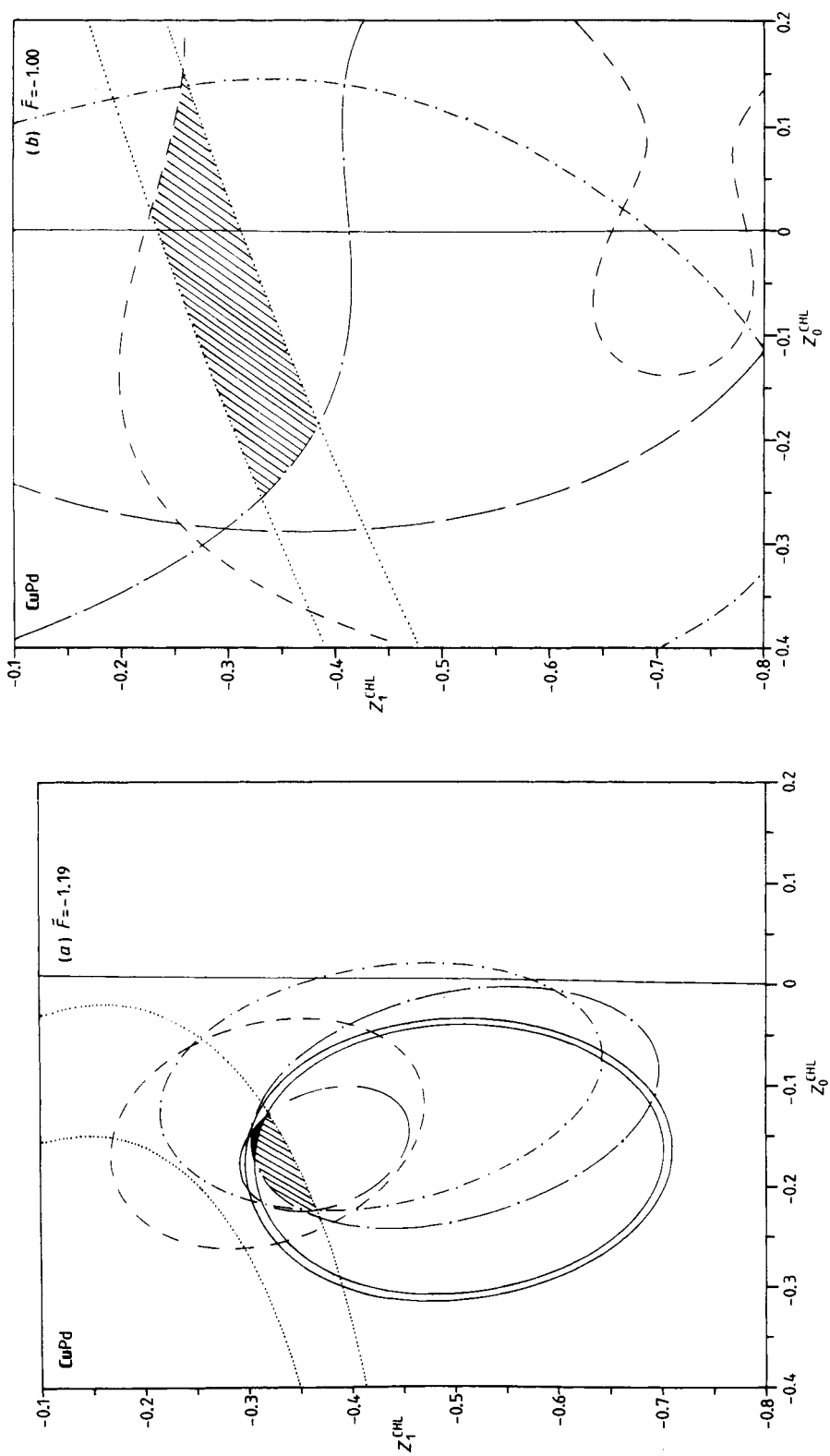

Figure 10. (*a*) **CuPd**: computed loci of constant values of X and $\Delta\rho/c$ (band between full curves) in the CHL model for $\tilde{F}=\tilde{F}_{\text{Blatt}}=-1.19$. The orbits are as in figure 9 and B_{111} (— · — ·). (*b*) **CuPd**: computed loci of constant values of ΔF in the CHL model for $\tilde{F}=\Delta Z=-1.00$. The orbits are as in figure 9 and B_{111} (— · — ·).

The analysis of Dingle temperatures shows a pronounced d phase shift with substantial s and p phase-shift contributions.

5.2. *CuPd*

The residual resistivity used in the present work ($0.82\ \mu\Omega$ cm (at.%)$^{-1}$) differs from that used by CTT ($0.89\ \mu\Omega$ cm (at.%)$^{-1}$). For $\tilde{F}_{\text{Blatt}}$ the Dingle temperatures gave a small region on the Z_0, Z_1 plots over which solutions exist. Within this range the Z_l values also represent $\Delta\rho/c$ in the CHL model (table 6). Solutions for all orbits were obtained for the Friedel sum range $-1.20 < \tilde{F} < -0.20$ (table 5). The regions of solutions in the Z_0, Z_1 plots split into two branches, giving solutions α'' and β'' for $\tilde{F} \geqslant -1.13$. (Solution α'' is the one with the most negative s component and the most positive d component.) A range of solutions also exists which, in addition to the Dingle temperatures, represents $\Delta\rho/c$: $-1.20 < \tilde{F} < -1.14$.

The frequency changes for $\tilde{F} = -1$ gave broad ranges of solutions particularly for Z_0 (-0.27 to $+0.17_5$). Z_0, Z_1 plots for both Dingle temperatures and ΔF are shown in figure 10. An important thing to note is that although it might seem from table 6 or figure 10 that there exists a common set of Z_l solutions to Dingle temperatures including resistivity and

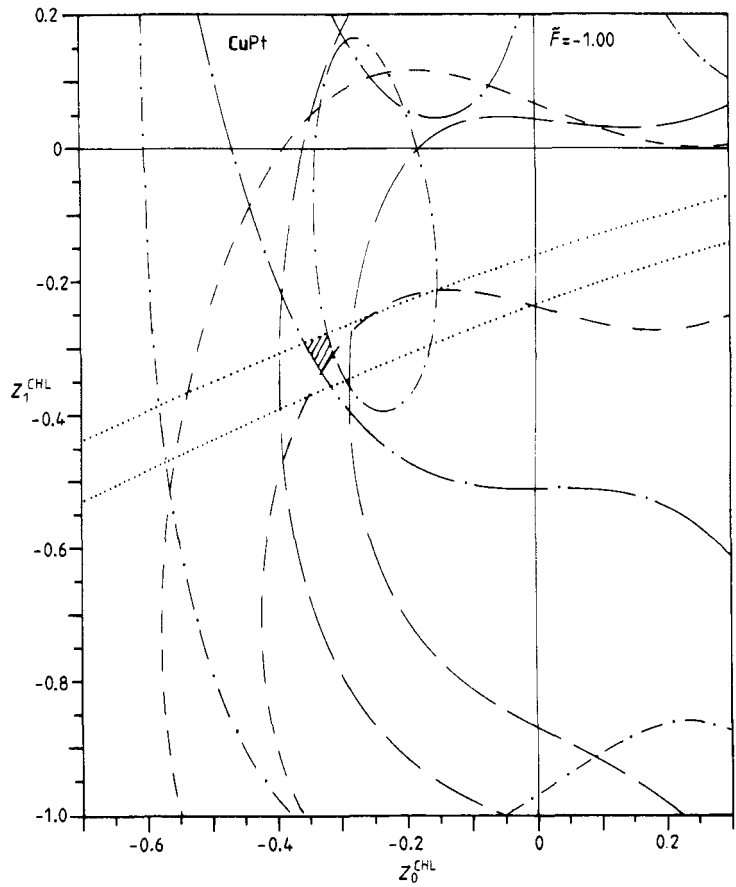

Figure 11. **Cu**Pt: computed loci of constant values of ΔF in the CHL model for $\tilde{F} = \Delta Z = -1.00$. The orbits are as in figure 9 and B_{111} (— · — ·).

frequency shifts, this is not the case since the sets are deduced for different Friedel sum values.

There is a dominant d contribution, though the s and p contributions are again appreciable.

5.3. CuPt

There is a considerable difference between the residual resistivity in the present work ($2.24\,\mu\Omega$ cm (at.%)$^{-1}$) and the value that CTT used ($2.10\,\mu\Omega$ cm (at.%)$^{-1}$). The solutions to the Dingle temperatures form two branches (α'', β'' in table 5), both extending over a wide range of Friedel sums. With the constraint of the residual resistivity the ranges of Friedel sums are considerably confined and no longer overlap. Solution β'' seems most likely because it gives a Friedel sum close to $\tilde{F}_{\text{Blatt}}$ when $(\Delta\rho/c)_{\text{CHL}}$ is included. For $\tilde{F}_{\text{Blatt}} = -1.20$ only solution α'' exists for the Dingle temperatures, but the residual resistivity value is far from the experimental value (table 6). We do not present a plot for any of these cases because the density of Dingle temperature curves in the Z_0, Z_1 plot was too high near the solution range to make them discernible. (The same holds for **Cu**Ni.)

The wide range of Friedel sums giving solutions for ΔF includes the value $\Delta Z = -1$ (table 5) and the Z_0, Z_1 plot is shown in figure 11. The Z_l values obtained in this case resemble those of type-α'' solutions for the Dingle temperatures (table 6). However, in both cases there is very poor agreement with the experimental residual resistivity. It is worthy of notice that, when comparing the type-β'' solutions of the Dingle temperatures including $(\Delta\rho/c)_{\text{CHL}}$ with the solution of the frequency changes (table 6), the Z_1 ranges agree very well whereas the Z_0 range of the latter is much more negative; this has the consequence that the $|Z_2|$ appear to be smaller.

5.4. CuRh

In this alloy the residual resistivity now used ($4.03\,\mu\Omega$ cm (at.%)$^{-1}$) again differs considerably from that used by CTT ($3.57\,\mu\Omega$ cm (at.%)$^{-1}$). There is no solution to the Dingle temperatures for $\tilde{F}_{\text{Blatt}} = -2.14$, but solutions are found for values of $\tilde{F}$ greater than -2.09; this is a more acceptable range of Friedel sums than obtained by CTT, -1.38 ± 0.4. Moreover, these solutions give values of $(\Delta\rho/c)_{\text{CHL}}$ which are in reasonable agreement with the experimental value as seen in table 6. For $\tilde{F} = -1.98$ even the experimental value of $\Delta\rho/c$ is reached. The Z_0, Z_1 plot for the Dingle temperatures is shown in figure 12. The solutions indicate a value of Z_2 of about -1.5, which is greater than that in **Cu**Ni, **Cu**Pd or **Cu**Pt in accordance with the resonant d-state picture. However, there are also obviously substantial s and p contributions to the Friedel sum.

The frequency changes give solutions at least over the range $-2.68 < \tilde{F} < -1.41$. Taking $\tilde{F} = -2$ gives the Z_l values shown in table 6, where it can be seen that the residual resistivity can be represented well by the solution. The above range of values of $\tilde{F}$ is again more acceptable than that of CTT, -1.38 ± 0.5, having regard to the value of ΔZ. The solution to ΔF for $\tilde{F} = \Delta Z = -2$ has the same value of Z_1 and a more negative value of Z_0 than the solution to X and $(\Delta\rho/c)_{\text{CHL}}$ for $\tilde{F} = -1.98$ (table 6), resulting in a smaller value of $|Z_2|$ as in the **Cu**Pt case.

In summary, the situation is that the phase shifts representing the Dingle temperatures and the frequency shifts are different; this partly reflects the different Friedel sums used. This difference is observed mainly in the s and d partial screening charges, $|Z_0|$ being greater and $|Z_2|$ smaller for the frequency changes than for the Dingle temperatures. In

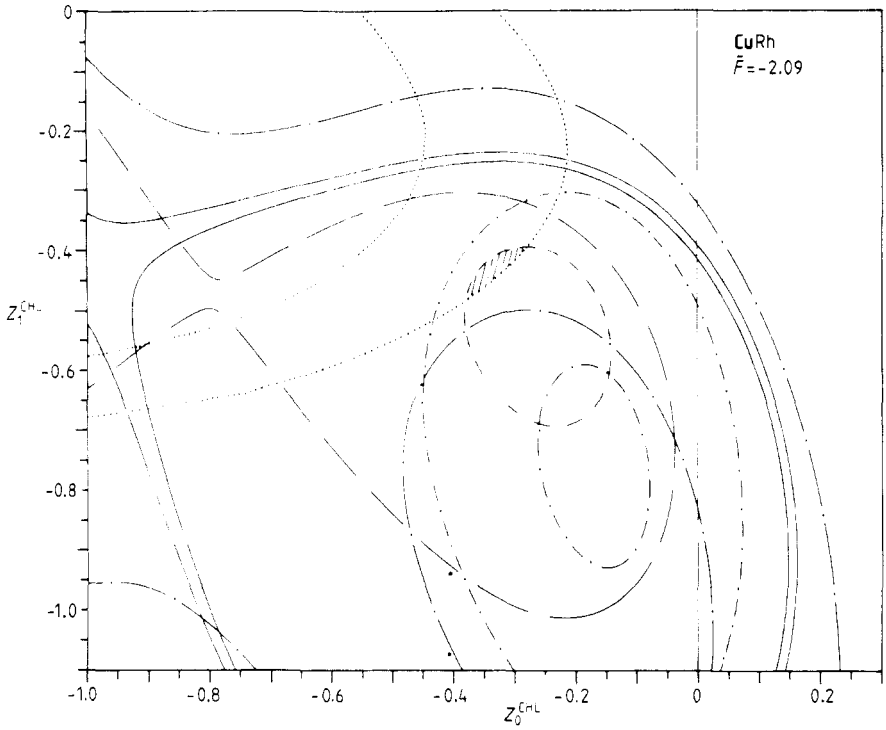

Figure 12. **Cu**Rh: computed loci of constant values of X and $\Delta\rho/c$ (band between full curves) in the CHL model for $\tilde{F}=-2.09$. The orbits are as in figure 9 and B_{111} (— · — ·).

making comparisons the Z_l^{GB} solutions obtained within the GB model should be compared with the Z_l^{CHL} solutions for X including $\Delta\rho/c$ obtained within the CHL model for $\tilde{F}\sim\tilde{F}_{Blatt}$, since scattering properties are sensitive to local lattice distortion. However, it should be pointed out that lattice distortion affects the resistivity and Dingle temperatures in different ways because of the different effect of small-angle scattering on both properties. For the **Cu**Pd system solutions are obtained for $\tilde{F}=\tilde{F}_{Blatt}$, but in the other three systems we had to use a slightly different Friedel sum.

6. Discussion

6.1. Comparison of the Z_l^{GB} and Z_l^{CHL} solutions

The Z_l^{GB} values in table 4(*a*) and the Z_l^{CHL} values in table 6 are given for a variety of Friedel sums for the reasons already indicated. It is essential in making comparisons between Z_l^{GB}, from resistivity and TEP measurements, and Z_l^{CHL}, from resistivity and Dingle temperature measurements, to do so for the same Friedel sum in each alloy system. (Comparison is made between these properties because they are all affected similarly, but perhaps not exactly in the same way, as mentioned above, by lattice distortion and charge transfer.) This has been done in figure 13. Examining the difference between the $\Delta\rho/c$ bands in the GB and CHL models for a particular alloy system shows clearly that the GB approximation fails for **Cu**Pd. For the other three systems, all with higher resistivity values than **Cu**Pd, the two curves are very much the same. It is important to note that the line at

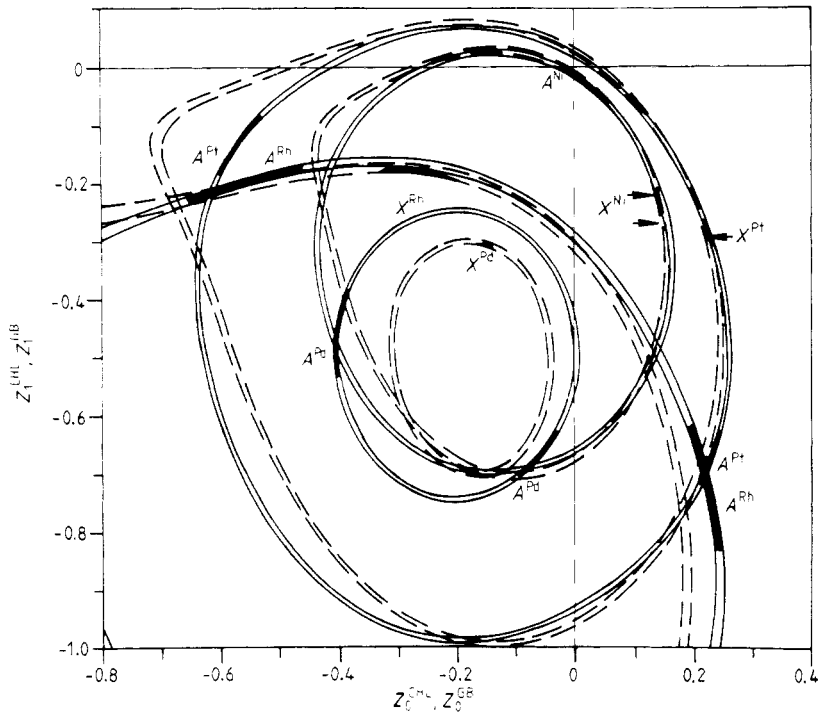

Figure 13. Computed loci of constant values of $\Delta\rho/c$ in the GB (full curves) and CHL (broken curves) models. The Friedel sums used for **Cu**Ni, **Cu**Pd, **Cu**Pt and **Cu**Rh are −0.80, −1.19, −1.08 and −1.98, respectively. The solutions for X and A are marked for each system.

−45° drawn in the figure corresponds to a value of Z_2 which depends on the alloy system because of the different Friedel sums employed for each alloy. It is clear from figure 13 that the solutions for **Cu**Pd, **Cu**Pt and **Cu**Rh for the Dingle temperatures all give a higher d contribution than the solution for the TEP. The opposite is the case for **Cu**Ni. We should recall that for **Cu**Pd, **Cu**Pt and **Cu**Rh the Z_2 values deduced from the UPS were in agreement with the values of Z_2^{GB} deduced from A and $\Delta\rho/c$ using E_d from the UPS, whereas for **Cu**Ni a considerable discrepancy was found (see §§ 4.1 and 4.2).

As far as obtaining better agreement is concerned, it should be realised that the neck plays a dominant role in determining the CHL solution while the TEP also plays a similar role in determining the solution in the GB model, but since this is based on a spherical band approximation improvement will be made only when the TEP can be introduced into the CHL model.

6.2. Comparison with theory

There are effects, such as charge transfer, that influence transport as well as DHVA properties in both models and it is therefore useful to compare the DHVA and resistivity measurements with the results of theoretical calculations. Several theoretical approaches have been followed, varying from *ab initio* calculations by Riedinger (1973), using a pseudopotential theory, to the elaborate description of scattering of Bloch electrons by a cluster consisting of an impurity together with one neighbouring shell of host atoms (Braspenning *et al* 1984). The latter theory is capable of taking into account charge-transfer effects between the impurity and the next-neighbouring host atoms. For the

calculation of $\Delta\rho/c$ a finite cluster model (FCM) is employed in which the cluster is embedded in free space (Lodder and Braspenning 1980). This is unlike the cluster calculations of DHVA properties which are made with a perfect lattice (Molenaar *et al* 1983, Molenaar and Lodder 1983). Recently Mertig *et al* (1983a, b, c) have calculated Dingle temperatures, frequency shifts and resistivities of 4d transition impurities in a Cu host using self-consistently determined host and single-site impurity potentials. Their calculations were based on a muffin-tin approximation and a self-consistent KKR description of the host, assuming that only the potential within the impurity Wigner–Seitz sphere is perturbed. In two earlier papers Mertig and Mrosan (1980, 1982) investigated the influence of 3d impurities in Cu on the DHVA effect, starting from a model impurity potential of the muffin-tin type determined using the Friedel sum rule and a non-self-consistent treatment of the host band structure in terms of a linearised KKR version of hybridised NFE tight binding. Mertig *et al* (1982, 1983b) calculated $\Delta\rho/c$ taking into account the anisotropy of the scattering potential as well as the anisotropy of the Fermi surface, using an exact solution of the Boltzmann equation. We have used their single-site potential phase shifts to calculate $\Delta\rho/c$ in the GB model (equation (5)). It should be pointed out that these values differ slightly from their quoted values because a different Fermi energy in the prefactor of (5) has been used. Comparing the results of single-site and cluster calculations (Lodder 1983) with the experimental values for X, $(1/c)\Delta F/F_s$ and $\Delta\rho/c$ for **Cu**Ni, **Cu**Pd and **Cu**Rh (tables 7–9) gives insight into the importance of charge transfer in these systems.

In **Cu**Ni the Dingle temperatures calculated by Mertig and Mrosan (1980) using a non-self-consistent host description are in far better agreement with experiment than the results of Lodder (1983), who used cluster potentials determined self-consistently. Braspenning *et al* (1984) showed that charge transfer is a minor effect in this system and the reason for the difference between the theoretical calculations could be the better description of the host anisotropy in the calculation by Mertig and Mrosan (1980); this was found to be important for sp impurities in Cu by Molenaar *et al* (1983).

As far as the frequency shifts are concerned, since the calculations do not take lattice distortion into account the theoretical values are compared with the experimental values

Table 7. Dingle temperatures $X(\omega)/c$ for **Cu**Ni, **Cu**Pd and **Cu**Rh. Units are K (at.%)$^{-1}$. $\tilde{F}$ is the Friedel sum.

Alloy system	Reference	ω					
		B_{111}	B_{100}	N_{111}	D_{110}	R_{100}	$\tilde{F}$
CuNi	Expt[a]	30.9 ± 2.0	26.6 ± 1.9	14.9 ± 1.8	26.6 ± 2.5	25.0 ± 1.5	
	Theory[c]	24.8	21.2	14.5	18.4	20.9	−1.01
	Theory[d]	32.5	28.0	10.8	24.2	27.4	−1.00
CuPd	Expt[b]	32.0 ± 2.3	32.3 ± 2.3	$19.4_4 \pm 2.1_6$	28.7 ± 2.3	$28.6 \pm 2.4_4$	
	Theory[c]	32.4	31.2	22.6	26.8	27.9	−0.98
	Theory[e]	21.8	21.4	18.2	20.3	21.1	−0.89
CuRh	Expt[b]	119.5 ± 15.5	100.2 ± 6.6	47.1 ± 5.8	80.6 ± 7.2	90.0 ± 10.4	
	Theory[c]	123.0	110.1	76.4	95.0	104.4	−2.01
	Theory[e]	87.8	80.4	58.6	74.4	82.5	−1.70

[a] Poulsen *et al* (1974); [b] renormalised data of Coleridge *et al* (1981); [c] Lodder (1983); [d] Mertig and Mrosan (1980); [e] Mertig *et al* (1983c).

Table 8. Frequency shifts $(1/c)\Delta F(\omega)/F_s$ for **Cu**Ni, **Cu**Pd and **Cu**Rh. Units are free-electron-sphere cross section per unit concentration.

Alloy system	Reference	ω				
		B_{111}	B_{100}	N_{111}	D_{110}	R_{100}
CuNi	Expt[a]†	-0.771 ± 0.018	-0.682 ± 0.026	-0.116 ± 0.008	$+0.532 \pm 0.009$	$+0.590 \pm 0.004$
	Theory[c]	-0.743	-0.656	-0.164	$+0.541$	$+0.607$
	Theory[d]	-0.766	-0.671	-0.106	$+0.554$	$+0.682$
CuPd	Expt[b]†	-0.71 ± 0.05	$-0.64_7 \pm 0.07$	-0.17 ± 0.01	$+0.57_4 \pm 0.03$	$+0.62 \pm 0.04$
	Theory[c]	-0.685	-0.627	-0.161	$+0.519$	$+0.565$
	Theory[e]	-0.741	-0.712	-0.194	$+0.607$	$+0.670$
CuRh	Expt[b]†	-1.06 ± 0.09	-0.86 ± 0.07	-0.21 ± 0.03	$+0.82_2 \pm 0.09$	$+0.89 \pm 0.08$
	Theory[c]	-1.276	-1.141	-0.284	$+0.938$	$+1.042$
	Theory[e]	-1.367	-1.265	-0.317	$+1.063$	$+1.211$

[a] Templeton and Coleridge (1975); [b] renormalised data of Coleridge *et al* (1981); [c] Lodder (1983); [d] Mertig and Mrosan (1982); [e] Mertig *et al* (1983c).
† Corrected for lattice expansion.

corrected for long-range lattice distortion. The frequency shifts calculated by Lodder for the N_{111}, B_{111} and R_{100} orbits lie outside the experimental uncertainties. (The B_{111} orbit lay outside the common region of intersection in the earlier analysis of the experimental data.) The non-self-consistent potentials of Mertig *et al* (1982) give excellent agreement for the electron orbits but are less satisfactory in describing the hole orbits.

The experimental $\Delta\rho/c$ falls in between the single-site and cluster calculations.

In **Cu**Pd the self-consistent cluster calculations of Lodder show excellent agreement with the measured Dingle temperatures, whereas the self-consistent single-site impurity calculations by Mertig *et al* (1983c) give Dingle temperatures which are much too low, with the exception of the neck orbit. The difference between the two calculations points to an important influence of charge transfer in this system, which is in agreement with the findings of Braspenning *et al* (1984).

The frequency shift calculations give good agreement with experiment for the electron orbits, although the experimental uncertainties are much higher than for **Cu**Ni. The experimental frequency shifts of the hole orbits lie between the results of the calculations of Lodder and Mertig *et al.*

Table 9. Residual resistivity for **Cu**Ni, **Cu**Pd and **Cu**Rh.

	$\Delta\rho/c$ ($\mu\Omega$ cm (at.%)$^{-1}$)		
	CuNi	**Cu**Pd	**Cu**Rh
Experiment[a]	1.11	0.82	4.03
Finite cluster model[b]	0.89	0.78	3.68
Exact solution of the Boltzmann equation	1.25[c]	0.24[d]	1.59[d]
Gupta–Benedek model	1.30[e]	0.30[f]	1.86[f]

[a] This work; [b] Lodder (1983); [c] Mertig *et al* (1982); [d] Mertig *et al* (1983b); [e] phase shifts from Mertig *et al* (1982); [f] phase shifts from Mertig *et al* (1983a).

The FCM gives much better agreement with experiment than the single-site calculations of $\Delta\rho/c$, supporting the view that charge transfer is important in this system.

In **Cu**Rh the Dingle temperatures calculated by Lodder are systematically higher than the measured values, especially for the neck and dogsbone orbits. From the plot of Dingle temperatures against $\Delta\rho$ (see figure 2 of CTT) these two orbits have the largest unphysical intercepts. Forcing the fits for these curves through the origin results in higher values of X. The fact that the calculated values for the dogsbone and especially the neck orbits are higher than the measured values could mean that the overall agreement is better. The large difference between the experimental results and the calculated values of Mertig *et al* (1983c) again points to strong charge-transfer effects, in agreement with Braspenning *et al* (1984).

The cluster calculations for the frequency change and $\Delta\rho/c$ approximate to the experimental results better than the single-site calculations. This is probably also evidence that charge transfer is important in this system.

In table 9 it can be seen that the values of $\Delta\rho/c$ obtained from the GB model are in good agreement with the values obtained from an exact solution of the Boltzmann equation.

7. Conclusions

In this work an attempt is made to relate properties which depend on the resonant d state, for example (i) those which depend on states at ε_F—$\Delta\rho/c$, X/c and $(1/c)\Delta F/F_s$—and (ii) those which depend on states at or below ε_F—the UPS. In addition, the TEP is investigated since this forms a link between (i) and (ii), depending as it does on the way in which the states vary with energy at ε_F. For $\Delta\rho/c$, TEP and UPS a consistent picture arises from two different methods of analysis for the partial screening charges Z_l in the cases of Pd, Pt and Rh impurities in Cu. The case of **Cu**Ni is very interesting; partial screening charges derived with the two methods are considerably different, pointing to the need for a theory which includes electron–electron correlations.

Comparing the partial screening charges as derived from the transport and DHVA properties has led to difficulties because different models are used in their analysis and in the case where two models are able to account for the same property, the GB and CHL models for $\Delta\rho/c$, rather different solutions can be produced. It is also important to stress that the models are of varying sophistication as far as the assumption of real metal properties is concerned, ranging from the spherical-band GB model with a spherical Fermi surface to the KKR representation used with the full Fermi surface topology in the CHL model. The need for a theory covering both transport and DHVA is evident.

As far as the theoretical work is concerned, considerable progress has been made in calculations, some of which are from first principles. In some cases charge transfer is obviously playing a significant role.

Acknowledgments

It is a pleasure to acknowledge the interest and advice of Professor P F de Châtel and Professor G A Sawatzky at various stages in this work. We are indebted to Professor A Lodder for sending us his unpublished cluster calculations and for useful discussions.

References

Anderson P W 1961 *Phys. Rev.* **124** 41–53

van Baarle C, Gorter F W and Winsemius P 1967 *Physica* **35** 223–40

Bass J and Fischer K H 1982 *Numerical Data and Functional Relationships in Science and Technology, Group III: Crystal and Solid State Pysics* vol. 15 *(Metals: Electronic Transport Phenomena)* subvol. a (Berlin: Springer)

Beaglehole D 1976 *Phys. Rev.* B **14** 341–6

Blatt F J 1957 *Phys. Rev.* **108** 285–90

Blatt F J, Schroeder P A, Foiles C L and Greig D 1976 *Thermoelectric Power of Metals* (New York: Plenum) p 208

Bosch A 1982 *Thesis* University of Groningen

Bosch A, Feil H, Sawatzky G A and Julianus J A 1984 *J. Phys. F: Met. Phys.* **14** 2225–38

Braspenning P J, Zeller R, Lodder A and Dederichs P H 1984 *Phys. Rev.* B **29** 703–18

Clogston A M 1961 *Phys. Rev.* **125** 439–43

Coleridge P T 1975 *J. Phys. F: Met. Phys.* **5** 1317–26

Coleridge P T, Holzwarth N A W and Lee M J G 1974 *Phys. Rev.* B **10** 1213–29

Coleridge P T, Templeton I M and Toyoda T 1981 *J. Phys. F: Met. Phys.* **11** 2345–57

Daniel E and Friedel J 1965 *Low Temperature Physics—LT 9* (New York: Plenum) pp 933–54

Friedel J 1958 *Nuovo Cimento* **7** 287–311

Gardner J L and Samson J A R 1975 *J. Electron Spectrosc. Rel. Phen.* **6** 53

Gold A V, MacDonald D K C, Pearson W B and Templeton I M 1960 *Phil. Mag.* **50** 765–83

Guénault A M 1967 *Phil. Mag.* **15** 17–25

—— 1974 *J. Phys. F: Met. Phys.* **4** 256–67

Guénault A M and Lawson N S 1981 *J. Phys. F: Met. Phys.* **11** 2139–45

Gupta R P and Benedek R 1979 *Phys. Rev.* **19** 583–6

Guthrie G L, Friedberg S A and Goldman J E 1959 *Phys. Rev.* **113** 45–8

Julianus J A, Bekker F F and de Châtel 1984a *J. Phys. F: Met. Phys.* **14** 2061–76

—— 1984b *J. Phys. F: Met. Phys.* **14** 2077–86

Kierspe W 1967 *Z. Metallk.* **58** 895–902

Kondo J 1965 *Prog. Theor. Phys.* **34** 372–82

Lee M J G, Holzwarth N A W and Coleridge P T 1976 *Phys. Rev.* B **13** 3249–60

Legvold S, Peterson D T, Burgardt P, Hofer R J, Lundell B, Vyrostek T A and Gärtner H 1974 *Phys. Rev.* B **9** 2386–9

Lengeler B, Schilling W and Wenzl H 1970 *J. Low-Temp. Phys.* **2** 59–86

Lengeler B, Wampler W R, Bourassa R R, Mika K, Wingerath K and Uelhoff W 1977 *Phys. Rev.* B **15** 5493–503

Linde J O 1932 *Ann. Phys., Lpz* **15** 219

Lodder A 1983 Private communication

Lodder A and Braspenning P 1980 *J. Phys. F: Met. Phys.* **10** 2259–77

Loegel B 1973 *J. Phys. F: Met. Phys.* **3** L106–9

McLachlan A D, Jenkin J G, Leckey R C G and Liesegang J 1975 *J. Phys. F: Met. Phys.* **5** 2415–23

van der Marel D, Sawatzky G A and Julianus J A 1985 to be published

Mertig I and Mrosan E 1980 *J. Phys. F: Met. Phys.* **10** 417–25

—— 1982 *J. Phys. F: Met. Phys.* **12** 1139–42

Mertig I, Mrosan E and Schöpke R 1982 *J. Phys. F: Met. Phys.* **12** 1689–96

Mertig I, Mrosan E, Zeller R and Dederichs P H 1983b *Phys. Status Solidi* b **117** 619–23

—— 1983c *Phys. Status Solidi* b **119** 251–60

Mertig I, Mrosan E, Zeller R, Dederichs P H and Ziesche P 1983a *Phys. Status Solidi* b **117** 335–44

Molenaar J and Lodder A 1983 *J. Phys. F: Met. Phys.* **13** 1501–10

Molenaar J, Lodder A and Coleridge P T 1983 *J. Phys. F: Met. Phys.* **13** 839–55

Moruzzi V L, Janak J F and Williams A R 1978 *Calculated Electronic Properties of Metals* (New York: Pergamon)

Myers A, Bekker F F and van Nassou H 1980 *J. Phys. F: Met. Phys.* **10** 461–9

Pearson W B 1958 *A Handbook of Lattice Spacings and Structures of Metals and Alloys* (New York: Academic) pp 595–601 (see also 1967 vol. 2 p 881)

Pemberton I and Guénault A M 1971 *Phys. Lett.* **37A** 17–8

Podloucky R, Zeller R and Dederichs P H 1980 *Phys. Rev.* B **22** 5777–90

Poulsen R G, Randles D L and Springford M 1974 *J. Phys. F: Met. Phys.* **4** 981–99
Riedinger R 1973 *J. Phys. F: Met. Phys.* **3** 967–76
Schöpke R and Mrosan E 1978 *Phys. Status Solidi* b **90** K95–8
Schroeder P A, Wolf R and Woollam J A 1965 *Phys. Rev.* **138** A105–11
Templeton I M and Coleridge P T 1975 *J. Phys. F: Met. Phys.* **5** 1307–16
Zeller R and Dederichs P H 1979 *Phys. Rev. Lett.* **42** 1713–6
Zeller R, Podloucky R and Dederichs P H 1980 *Z. Phys.* B **38** 165–8